Article

SOURCE DATA | TRANSPARENT PROCESS | OPEN ACCESS

EMBO reports

BAZ2A-mediated repression via H3K14ac-marked enhancers promotes prostate cancer stem cells

Rodrigo Peña-Hernández[1,2], Rossana Aprigliano[1], Sandra Carina Frommel[1], Karolina Pietrzak[1,2], Seraina Steiger[1], Marcin Roganowicz[1,3], Luigi Lerra[1,3], Juliana Bizzarro[1] & Raffaella Santoro[1,*]

Abstract

Prostate cancer (PCa) is one of the most prevalent cancers in men. Cancer stem cells are thought to be associated with PCa relapse. Here, we show that BAZ2A is required for PCa cells with a cancer stem-like state. BAZ2A genomic occupancy in PCa cells coincides with H3K14ac-enriched chromatin regions. This association is mediated by BAZ2A-bromodomain (BAZ2A-BRD) that specifically binds H3K14ac. BAZ2A associates with inactive enhancers marked by H3K14ac and repressing transcription of genes frequently silenced in aggressive and poorly differentiated PCa. BAZ2A-mediated repression is also linked to EP300 that acetylates H3K14ac. BAZ2A-BRD mutations or treatment with inhibitors abrogating BAZ2A-BRD/H3K14ac interaction impair PCa stem cells. Furthermore, pharmacological inactivation of BAZ2A-BRD impairs *Pten*-loss oncogenic transformation of prostate organoids. Our findings indicate a role of BAZ2A-BRD in PCa stem cell features and suggest potential epigenetic-reader therapeutic strategies to target BAZ2A in aggressive PCa.

Keywords BAZ2A; bromodomain; chromatin; H3K14ac; prostate cancer
Subject Categories Cancer; Chromatin, Transcription & Genomics; Signal Transduction
DOI 10.15252/embr.202153014 | Received 6 April 2021 | Revised 29 July 2021 | Accepted 2 August 2021 | Published online 17 August 2021
EMBO Reports (2021) 22: e53014

Introduction

Tumors are composed of heterogeneous populations of cells, which differ in their phenotypic and genetic features (Saygin *et al*, 2019). It has been suggested that cellular heterogeneity within a tumor is organized in hierarchical manner with a subpopulation of cancer stem cells (CSC) that give rise to heterogeneous cancer cell lineages and undergo self-renewal to maintain their reservoir (Pattabiraman & Weinberg, 2014). Furthermore, non-stem, differentiated cancer cells can transit into a dedifferentiated, CSC-like phenotype (Plaks *et al*, 2015; Rich, 2016). CSCs were shown to have an enhanced capacity for therapeutic resistance, immune evasion, invasion, and metastasis (Prager *et al*, 2019). Thus, efficient targeting of CSCs in cancer treatment is critical for developing effective therapeutics.

Prostate cancer (PCa) is the second most common epithelial cancer and the fifth leading cause of cancer-related death in men worldwide (Bray *et al*, 2018). PCa displays a high heterogeneity that leads to distinct histopathological and molecular features (Li & Shen, 2018). This heterogeneity posits one of the most confounding and complex factors underlying its diagnosis, prognosis, and treatment (Yadav *et al*, 2018). Current therapeutic approaches for PCa remain insufficient for some patients with progressive disease. Targeting of the androgen receptor (AR) axis through androgen ablation therapy and/or AR antagonists (castration) in patients with PCa relapse was shown to be efficient only for a short period of time (Denmeade & Isaacs, 2002). These treatments are not curative; a population of cells resistant to androgen-deprivation therapy emerges and PCa becomes unresponsive and progresses to a castrate-resistant prostate cancer (CRPC) and metastasis, with limited treatment options (Linder *et al*, 2018). Due to the enticing possibility that PCa aggressiveness and relapse arises from PCa stem cells (Colombel *et al*, 2012; Seiler *et al*, 2013; Mayer *et al*, 2015), the development of stem cell-specific anticancer drugs constitutes an attempt to innovate in the treatment of PCa (Leão *et al*, 2017).

Targeting of bromodomain (BRD)-containing proteins is a promising therapeutic approach, currently undergoing clinical evaluation in CRPC patients (Welti *et al*, 2018). Bromodomain-containing proteins regulate gene expression primarily through recognition of histone acetyl residues, leading to the recruitment of protein complexes that modulate gene expression (Fujisawa & Filippakopoulos, 2017). Bromodomain-containing proteins are frequently deregulated in cancer, and the development of BRD inhibitors as anticancer agents is now an intense area of research (Fujisawa & Filippakopoulos, 2017). JQ1, an inhibitor of proteins belonging to bromodomain and extraterminal domain (BET) family, has an effect in AR-signaling-competent human CRPC cell lines, whereas in AR-independent cell lines, such as PC3 cells, these inhibitors do not display any effect (Asangani *et al*, 2014).

BAZ2A (also known as TIP5) is a bromodomain-containing protein and subunit of the nucleolar-remodeling complex NoRC (Santoro *et al*, 2002; Zhou & Grummt, 2005). Recent work

1 Department of Molecular Mechanisms of Disease, DMMD, University of Zurich, Zurich, Switzerland
2 Molecular Life Science Program, Life Science Zurich Graduate School, University of Zurich, Zurich, Switzerland
3 RNA Biology Program, Life Science Zurich Graduate School, University of Zurich, Zurich, Switzerland
*Corresponding author. Tel: +41 44 6355475; E-mail: raffaella.santoro@dmmd.uzh.ch

implicated BAZ2A in aggressive PCa. BAZ2A is highly expressed in metastatic tumors compared with primary and localized tumors, required for cell proliferation, viability, and invasion, and represses genes frequently silenced in aggressive PCa (Gu *et al*, 2015). Furthermore, high BAZ2A levels in tumors associate with poor prognosis and disease recurrence. Finally, it was shown that BAZ2A is required for the initiation of PCa driven by *PTEN* loss, one of the most commonly lost tumor suppressor genes in PCa (Pietrzak *et al*, 2020).

BAZ2A contains a bromodomain that binds to acetylated histones (Zhou & Grummt, 2005; Tallant *et al*, 2015). In this work, we show that BAZ2A genomic occupancy in PCa cells coincides with H3K14ac-enriched chromatin regions. This association is mediated by BAZ2A-bromodomain, an epigenetic reader of H3K14ac. In PCa cells, BAZ2A-bromodomain is required for the interaction with a class of inactive enhancers that are marked by H3K14ac and represses the expression of genes implicated in developmental and differentiation processes that are linked to aggressive and dedifferentiated PCa. BAZ2A-mediated repression of these genes is also linked to the histone acetyltransferase EP300 that acetylates H3K14ac and displays the highest positive correlation with BAZ2A expression in both metastatic and primary tumors compared with the other H3K14 acetyltransferases. Mutations of BAZ2A-bromodomain or treatment with chemical probes that abrogate BAZ2A-bromodomain association with H3K14ac impair PCa stem cells. Furthermore, pharmacological inactivation of BAZ2A-bromodomain impairs the oncogenic transformation mediated by *Pten* loss in PCa organoids. Our findings indicate that BAZ2A is a key player in PCa stem cell features and suggest potential epigenetic-reader therapeutic strategies to target BAZ2A-bromodomain in aggressive, poorly differentiated PCa.

Results

BAZ2A associates with chromatin regions marked by H3K14ac

To determine whether BAZ2A-bromodomain is implicated in BAZ2A-mediated regulation of PCa, we investigated its genomic occupancy and the correlation with histone marks in metastatic PCa PC3 cells. We performed ChIPseq analysis of PC3 cells transfected with plasmids expressing HA-tagged BAZ2A and found 96,351 regions that were bound by BAZ2A (Fig 1A). We validated these results by ChIP-qPCR through the measurement of the binding of endogenous BAZ2A with two selected genes (*AOX1,* that as described below is a gene directly regulated by BAZ2A, and *EVX2*) using a PC3 cell line that expresses endogenous BAZ2A with a FLAG-HA (F/H) tag at the N-terminus (Figs 1B and C, and EV1A and B). The correlation between ChIPseq signal enrichment for BAZ2A binding and histone marks in PC3 cells indicated that BAZ2A has the strongest association with H3K14ac whereas its interaction with H3K27ac regions was much weaker (Fig 1A, B and D). To determine whether BAZ2A-bromodomain specifically recognizes H3K14ac, we used histone peptide arrays containing 384 unique histone modification combinations that allow the analysis of not only individual modified residues but also the effects of neighboring modifications (Figs 1E and EV1C). We incubated purified recombinant human BAZ2A-bromodomain fused to GST tag with the histone array and monitored the binding to histone peptides using anti-GST antibodies. Consistent with previous results (Zhou & Grummt, 2005; Tallant *et al*, 2015), BAZ2A-bromodomain did not interact with unmodified histone peptides and showed a preferential binding to a specific set of acetylated histone peptides. In line with the ChIPseq analyses, the acetylation per se was not sufficient for the binding of BAZ2A-bromodomain as evident by the lack of interaction with acetylated histone peptides such as H3K27ac. Interestingly, H3K14ac peptide was the mono-acetylated histone peptide displaying the highest interaction with BAZ2A-bromodomain, a result that is consistent with the ChIPseq analysis. Phosphorylation of H3S10 or acetylation of H3K9 improved the interaction of BAZ2A with H3K14ac. Poly-acetylated histone H4 containing K5ac, K8ac, K12ac, and K16ac was also a good target for BAZ2A-bromodomain whereas the interaction with these single H4 acetylated residues was much weaker or even absent as in the case of H4K5ac. To further support the specificity of BAZ2A-bromodomain as reader of H3K14ac, we mutated BAZ2A-Y1830 and N1873, which recent structural analyses indicated as critical residues for the interaction of BAZ2A-bromodomain with acetylated histones (Tallant *et al*, 2015). Accordingly, the interaction of both BAZ2A-BRD_{Y1830F} and BAZ2A-BRD_{N1873L} with modified histone peptides was strongly reduced, particularly for the mono-acetylated H3K14ac peptide (Fig 1E).

To determine whether BAZ2A-bromodomain mediates the association of BAZ2A with chromatin, we performed ChIPseq analysis of PC3 cells expressing murine BAZ2A mutated at the bromodomain HA-$BAZ2A_{Y1775F}$, an orthologous to the human BAZ2A-BRD_{Y1830F} unable to bind to acetylated histones (Zhou & Grummt, 2005). Equal expression of HA-$BAZ2A_{wt}$ and HA-$BAZ2A_{Y1775F}$ was assessed by Western blot (Fig EV1D). We found that only 1.3% (1534 peaks) of BAZ2A-bound sites were also occupied by $BAZ2A_{Y1775F}$, indicating that a functional bromodomain domain is required for BAZ2A binding to chromatin in PC3 cells (Figs 1A and F, and EV1E). Furthermore, the few DNA regions that retained binding with BAZ2A-bromodomain mutant contained low H3K14ac levels (Figs 1G and EV1F). Together, these results suggest that BAZ2A is an epigenetic reader of H3K14ac. Moreover, they show that in PC3 cells BAZ2A preferentially binds to regions marked by H3K14ac and that this interaction is mediated by BAZ2A-bromodomain.

BAZ2A binds to inactive enhancers marked by H3K14ac and mediates the repression of genes linked to developmental and differentiation processes

Previous studies showed that acetylation of H3K14 is mediated by histone acetyltransferases (HATs) EP300, KAT2A (GCN5), or KAT6A (Myst3) (Lee & Workman, 2007; Jin *et al*, 2011). Interestingly, we found that all these HATs are highly expressed in metastatic prostate cancer (Fig EV2A). In PC3 cells, however, only EP300 and KAT6A are expressed whereas *KAT2A* sequences are deleted (Seim *et al*, 2017) (Fig EV2B). The expression profile of these HATs in a large cohort of primary PCa and metastatic CRPC (Cancer Genome Atlas Research Network, 2015; Robinson *et al*, 2015) revealed that the levels of EP300 had the highest positive correlation with BAZ2A expression in both metastatic and primary tumors compared with KAT2A and KAT6A, suggesting that EP300 might be functionally related to BAZ2A binding to H3K14ac chromatin and the regulation of gene expression in PCa (Figs 2A and EV2C). Treatment of PC3 cells with A-485, a selective catalytic EP300 inhibitor (Lasko *et al*, 2017), induced a decrease in H3K14ac levels,

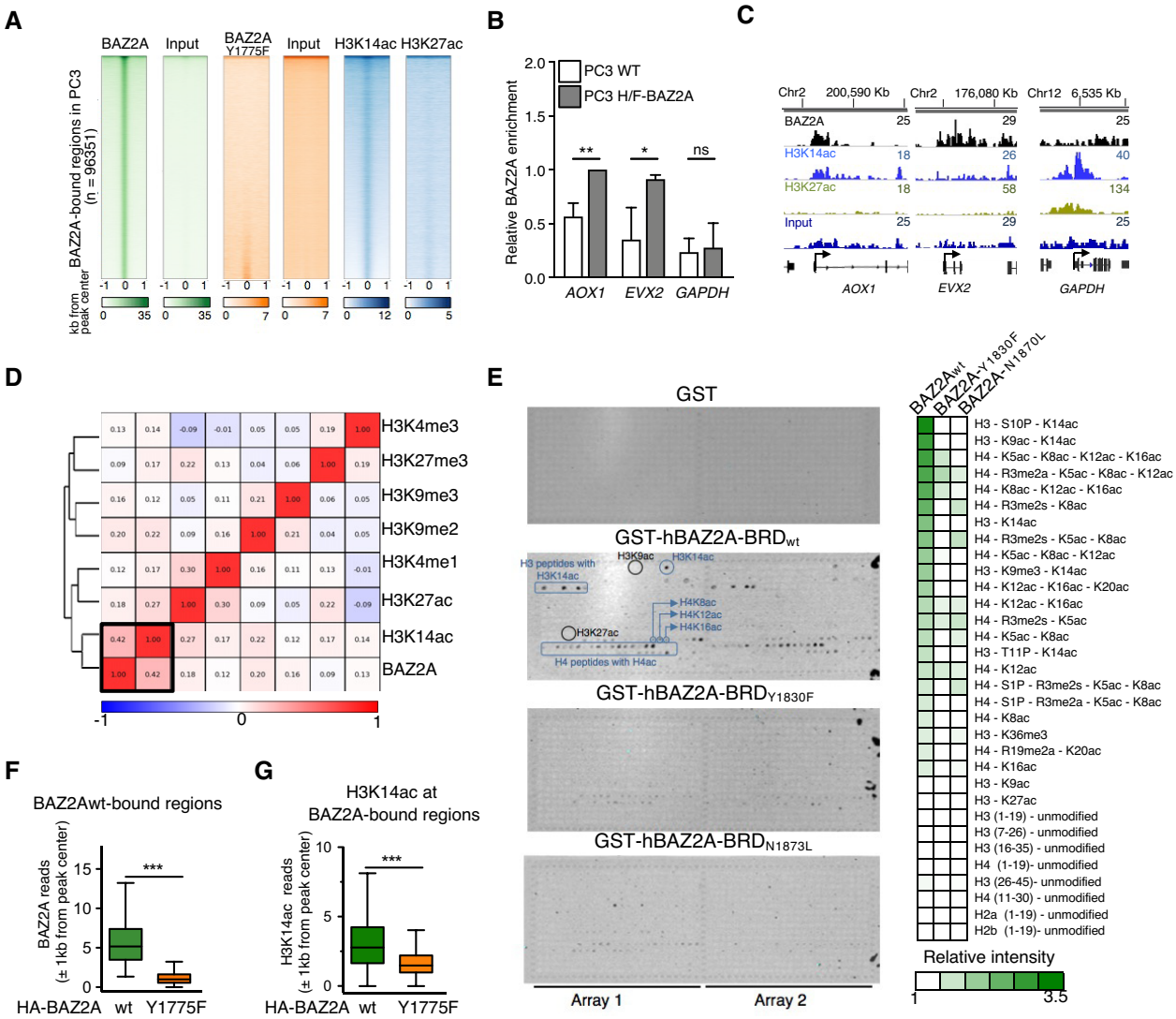

Figure 1. BAZ2A-bromodomain is an epigenetic reader of H3K14ac that mediates the BAZ2A association with H3K14ac-chromatin domains in PC3 cells.

A Heatmap profiles of BAZ2A-bound regions in PC3 cells and the corresponding signals of input, BAZ2A-bromodomain (BRD) mutant (Y1775F), H3K14ac, and H3K27ac. Data were ranked to BAZ2A binding in PC3 cells.

B Validation of ChIPseq results by anti-HA ChIP-qPCR of PC3 wild-type (WT) and a PC3 cell line that expresses endogenous BAZ2A with a FLAG-HA tag (PC3-H/F-BAZ2A). *GAPDH* promoter represents a region not bound by BAZ2A. Average values of three independent experiments. Data were normalized to input and to AOX1 levels. Statistical significance (*P*-values) was calculated using two-tailed *t*-test (*< 0.05, **< 0.001, ns: not significant). Error bars represent SD.

C Wiggle tracks displaying BAZ2A-bound regions, H3K14ac, H3K27ac, and input at *AOX1*, *EVX2*, and *GAPDH*.

D Pearson correlation heat map of BAZ2A-bound regions and histone marks. Data for BAZ2A, H3K4me3, H3K27me3, H3K27ac, and H3K14ac are from this work. H3K9me3, H3K9me2, and H3K4me1 were obtained from ENCODE.

E Images of histone peptide arrays probed with 10 nM of recombinant BAZ2A-BRD wild-type (GST-BAZ2A-BRD_{wt}) and mutants (GST-BAZ2A-BRD_{Y1830F} or GST-BAZ2A-BRD_{N1873L}). Visualization of binding was performed by incubation with anti-GST antibodies and imaged on Odyssey Infrared Imaging System. Blue circles mark peptides recognized by BAZ2A-BRD (i.e., H3K14ac), whereas black circles show some of the acetylated peptides not recognized by BAZ2A-BRD (H3K27ac and H3K9ac). Right panel shows heatmap of the relative binding intensity of BAZ2A-BRD against modified histone peptides. Binding intensity was calculated as average of fold change from peptides signal over background controls of two different arrays.

F BAZ2A read coverage quantification at ± 1 Kb from peak summit of BAZ2A-bound regions identified in PC3 cells and the corresponding reads for BAZ2A-BRD mutant (Y1775F) in PC3 cells. Statistical significance (*P*-values) was calculated using two-tailed *t*-test (***< 0.001).

G Regions bound by BAZ2A in PC3 cells are enriched in H3K14ac. Read coverage quantification for H3K14ac levels at regions bound by BAZ2A in PC3 cells (BAZ2Awt and BAZ2A-BRD mutant [Y1775F]) at ± 1 Kb from BAZ2A peak summits. Statistical significance (*P*-values) was calculated using two-tailed *t*-test (***< 0.001).

Data information: Boxplots in Fig 1 show the median and quartiles with the whiskers extending to the most extreme data point within 1.5 times the interquartile range.

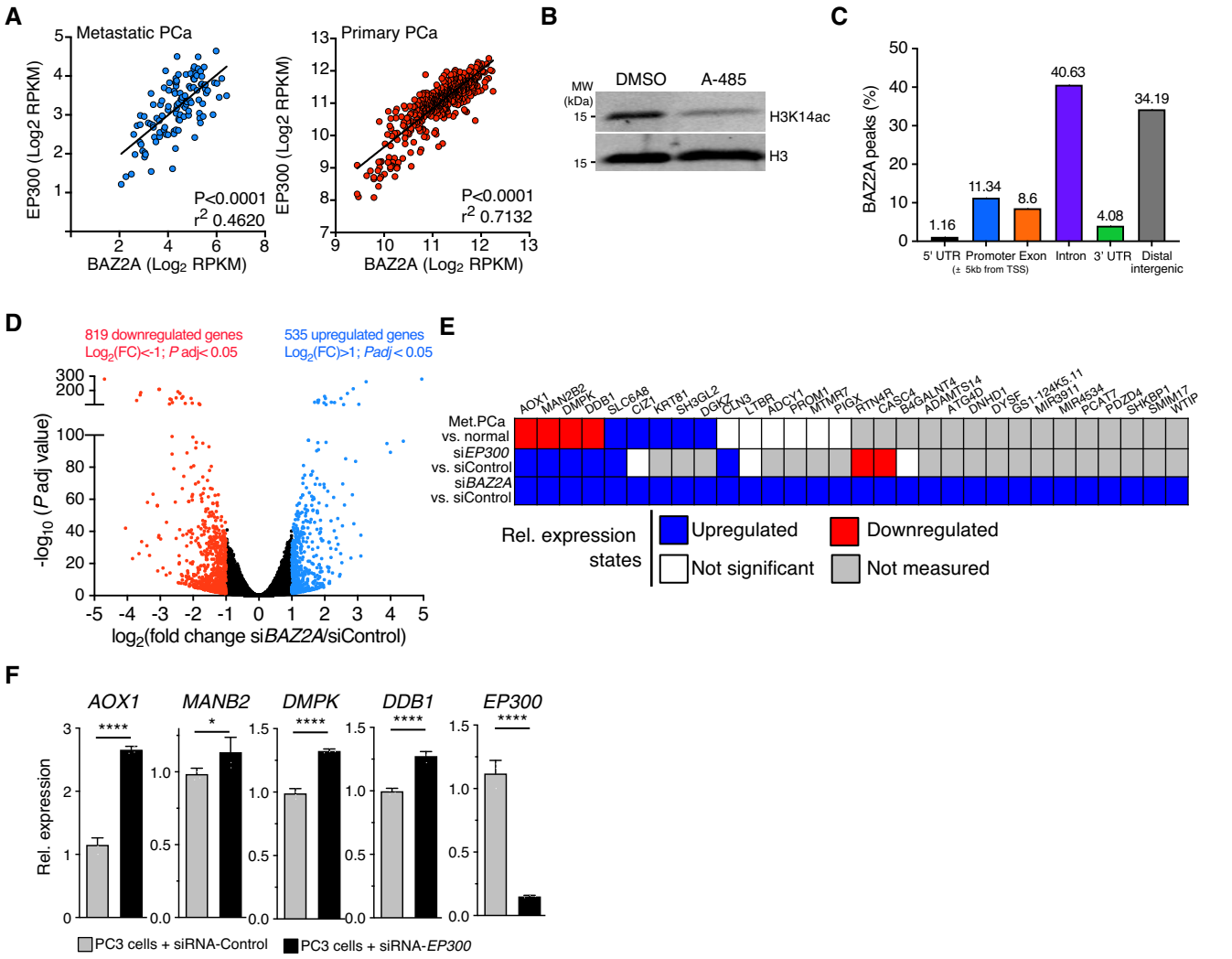

Figure 2. EP300-mediated acetylation of H4K14 mediates the repression of a set of genes with BAZ2A-bound promoter.

A Scatter plot showing the expression of *EP300* and *BAZ2A* in two large cohorts of metastatic and primary PCa. Data were from Cancer Genome Atlas Research Network (2015); Robinson *et al* (2015).

B EP300 acetylates H3K14 in PC3 cells. Western blot showing H3K14ac levels in PC3 cells treated for 3 days without and with the selective catalytic EP300 inhibitor A-485 (10 μM). Histone H3 serves as protein loading control.

C Genomic annotations of BAZ2A-bound regions in PC3 cells.

D Volcano plot showing fold change ($\log_2$ values) in transcript levels of PC3 cells upon BAZ2A knockdown. Gene expression values of two replicates were averaged and selected for 1.5-fold changes and $P < 0.05$.

E Table showing expression changes in genes with BAZ2A-bound promoter upregulated upon BAZ2A-KD in PC3 cells in metastatic PCa vs normal prostate tissue and in PC3 cells depleted of EP300 via siRNA.

F qRT–PCR showing increased expression levels of genes with BAZ2A-bound promoter and downregulated in metastatic tumors (*AOX1*, *MANB2*, *DMPK*, and *DDB1*—see (E)) in PC3 cells treated with siRNA-EP300.

Data information: Data were from three independent experiments. Values were normalized to *GAPDH* mRNA. Statistical significance (*P*-values) was calculated using two-tailed *t*-test (*<0.05, ****< 0.0001). Error bars represent SD.
Source data are available online for this figure.

confirming the role of EP300 in acetylating H3K14 (Fig 2B). To test the functional link between BAZ2A and EP300, we initially performed genomic annotation analyses of the BAZ2A-bound sites obtained with the BAZ2A-ChIPseq analysis. We found that BAZ2A peaks were mainly located in intronic or intergenic regions, whereas only a small fraction (11%) was located at gene promoters (Fig 2C). To determine which of the genes with BAZ2A-bound promoter transcriptionally depend on BAZ2A, we performed RNAseq of PC3 cells depleted of BAZ2A by siRNA. Consistent with previous results (Gu *et al*, 2015), BAZ2A-KD affects gene expression in PC3 cells ($\log_2$ fold change $> \pm 1$; *Padj* < 0.05; 535 upregulated genes, 819 downregulated genes; Fig 2D, Dataset EV1). We applied high stringency parameters to define genes with BAZ2A-bound promoter (527 genes with BAZ2A peak within ± 2 kb from transcription start and

BAZ2A fold change over input ≥ 3). However, only a minority of these genes were affected upon BAZ2A depletion (30 up- and 25 downregulated; Dataset EV2). Although the interaction of BAZ2A with the promoter does not appear the most prominent mechanism for BAZ2A-mediated regulation in PC3 cells, we found that depletion of EP300 by siRNA significantly reactivated the expression of *AOX1*, *DDB1*, *MANB2*, and *DMPK* (Fig 2E and F). Interestingly, these are the only upregulated genes upon BAZ2A-KD with BAZ2A-bound promoter that are significantly lower expressed in metastatic PCa compared with normal prostate tissue (Figs 2E and EV2D). Furthermore, low expression of *AOX1* has recently been correlated with shorter time to biochemical recurrence of PCa (Li *et al*, 2018). These results indicate that EP300 is required for BAZ2A-mediated repression of a set of genes with BAZ2A-bound promoter that are implicated in metastatic PCa.

Given that a large fraction of BAZ2A-bound regions are intronic and intergenic, we asked whether BAZ2A could regulate gene expression through its association with enhancers. First, we classified annotated enhancers (Plaschkes *et al*, 2017) at intergenic regions according to histone marks and chromatin accessibility and found that a large fraction of H3K14ac peaks in PC3 cells are located at active enhancers marked by H3K27ac, H3K4me1, and DNase I hypersensitive sites (from here on named as enhancer class 1, C1; Fig 3A). However, this class of active enhancers was not bound by BAZ2A. Interestingly, we found that BAZ2A only associates with a class of enhancers (named as C2) that relative to C1 enhancers had higher H3K14ac and H3K27me3 levels, lower content of H3K27ac, and lacked H3K4me1 and DNase I hypersensitive sites (Fig 3A and B). These results suggest that in PC3 cells, BAZ2A binds to a class of inactive enhancers that is enriched in H3K14ac. To determine whether the binding of BAZ2A to C2 enhancers affects gene expression, we analyzed the expression levels of genes in the nearest linear proximity to BAZ2A-bound C2 enhancers upon BAZ2A-KD in PC3 cells (Fig 3C and D, Dataset EV3). We found that 56% of these genes (417 out of 747) were significantly affected in their expression upon BAZ2A depletion. Furthermore, the majority of these BAZ2A-regulated genes (254 genes, 61%) showed upregulation upon BAZ2A-KD, suggesting a major role of BAZ2A in repressing gene transcription through its interaction with C2 enhancers. Interestingly, the top 10 gene ontology (GO) terms of these BAZ2A-regulated genes were strongly linked to developmental and differentiation processes (Fig 3E). Histological grading from well-differentiated to poorly differentiated PCa measured by Gleason score marks the progression from low- to high-grade cancer (Ahmed *et al*, 2012). We set to identify BAZ2A-bound C2 enhancer regulated genes that were upregulated upon BAZ2A-KD and lower expressed in Gleason 9 and 10 tumors (advanced) compared with Gleason 6 tumors (indolent). Using these criteria, we found 25 genes (Figs 3F and EV2E). Since GO terms associated with these genes were linked to developmental and cellular growth pathways, we selected five genes (*KRT8*, *EVC*, *ITPKB*, *SH3BP4*, and *SUN2*) that were implicated in these processes and analyzed their expression upon EP300 depletion in PC3 cells (Fig 3G and H). We found that EP300-KD increased the expression of all the selected genes, a result that further supports the functional link between BAZ2A and EP300 in the regulation of gene expression in PCa cells.

Collectively, these results suggest that BAZ2A binds to inactive C2 enhancers containing H3K14ac and mediates the repression of genes linked to developmental and differentiation processes that are frequently silenced in aggressive and poorly differentiated tumors.

BAZ2A-bromodomain is required for PCa stem cells

Several studies have reported that non-stem, differentiated cancer cells can transit into a dedifferentiated, CSC-like phenotype (Plaks *et al*, 2015; Rich, 2016). The role of BAZ2A in modulating the expression of genes linked to developmental processes and frequently silenced in aggressive and poorly differentiated tumors prompted us to determine whether BAZ2A plays a role in PCa stem cells and whether this is mediated by BAZ2A-bromodomain. To study this, we analyzed PCa stem cells in PC3 cells by measuring the amounts of tumorspheres generated using serum-free medium and low attachment culture conditions (Li *et al*, 2008; Rajasekhar *et al*, 2011; Sheng *et al*, 2013; Portillo-Lara & Alvarez, 2015). The PCa sphere-formation assay is an *in vitro* method commonly used to identify cancer stem cell. In particular, PC3 cells were shown to contain a

Figure 3. The association of BAZ2A with a class of inactive enhancers marked by H3K14ac represses genes implicated in aggressive PCa.

A BAZ2A binds to a class of inactive enhancers marked by H3K14ac. Heat maps of BAZ2A, H3K14ac, H3K27ac, H3K4me1, and DNAseq signal at annotated intergenic enhancers are shown. Enhancer regions were clustered in 4 groups based on the presence (+) or absence (−) of H3K27ac and H3K4me1. C1 ($H3K27ac^{+}/H3K4me1^{+}$), C2 ($H3K27ac^{+}/H3K4me1^{-}$), C3 ($H3K27ac^{-}/H3K4me1^{+}$), and C4 ($H3K27ac^{-}/H3K4me1^{-}$).

B Inactive enhancers (C2) are enriched in H3K14ac and BAZ2A levels. Read coverage at enhancer classes C1 and C2 for BAZ2A, H3K14ac, H3K27ac, H3K4me1, and H3K27me3 at ± 1 Kb from annotated enhancer regions. Statistical significance (*P*-values) was calculated using two-tailed *t*-test (***< 0.001). Boxplots show the median and quartiles with the whiskers extending to the most extreme data point within 1.5 times the interquartile range.

C Pie charts showing the number of genes in the nearest linear genome proximity to BAZ2A-bound C2 enhancers and their expression changes upon BAZ2A-KD in PC3 cells.

D Wiggle tracks showing RNA levels in PC3 cells treated with siRNA-BAZ2A and occupancy of BAZ2A, H3K14ac, H3K27ac, and H3K4me1 at C2 enhancer and its nearest gene *CXCR4*.

E Top 10 biological process gene ontology (GO) terms as determined using DAVID 6.8 for genes in the nearest linear proximity to BAZ2A-bound C2 enhancers that are differentially expressed upon BAZ2A-KD in PC3 cells.

F Heatmap showing expression changes in BAZ2A-bound C2-enhancer genes that were both significantly upregulated upon BAZ2A-KD and lower expressed in Gleason 9 and 10 tumors (advanced) compared with Gleason 6 tumors (indolent). Values from tumors were from Cancer Genome Atlas Research Network (2015).

G GO terms associated with the genes listed in (F). Genes labeled in bold were analyzed in (H).

H qRT–PCR showing increased expression levels of BAZ2A-bound C2-enhancer genes in PC3 cells treated with siRNA-EP300.

Data information: Data were from three independent experiments. Downregulation of *EP300* expression is shown in Fig 2F. Values were normalized to *GAPDH* mRNA. Statistical significance (*P*-values) was calculated using two-tailed *t*-test (*< 0.05, **< 0.001). Error bars represent SD.

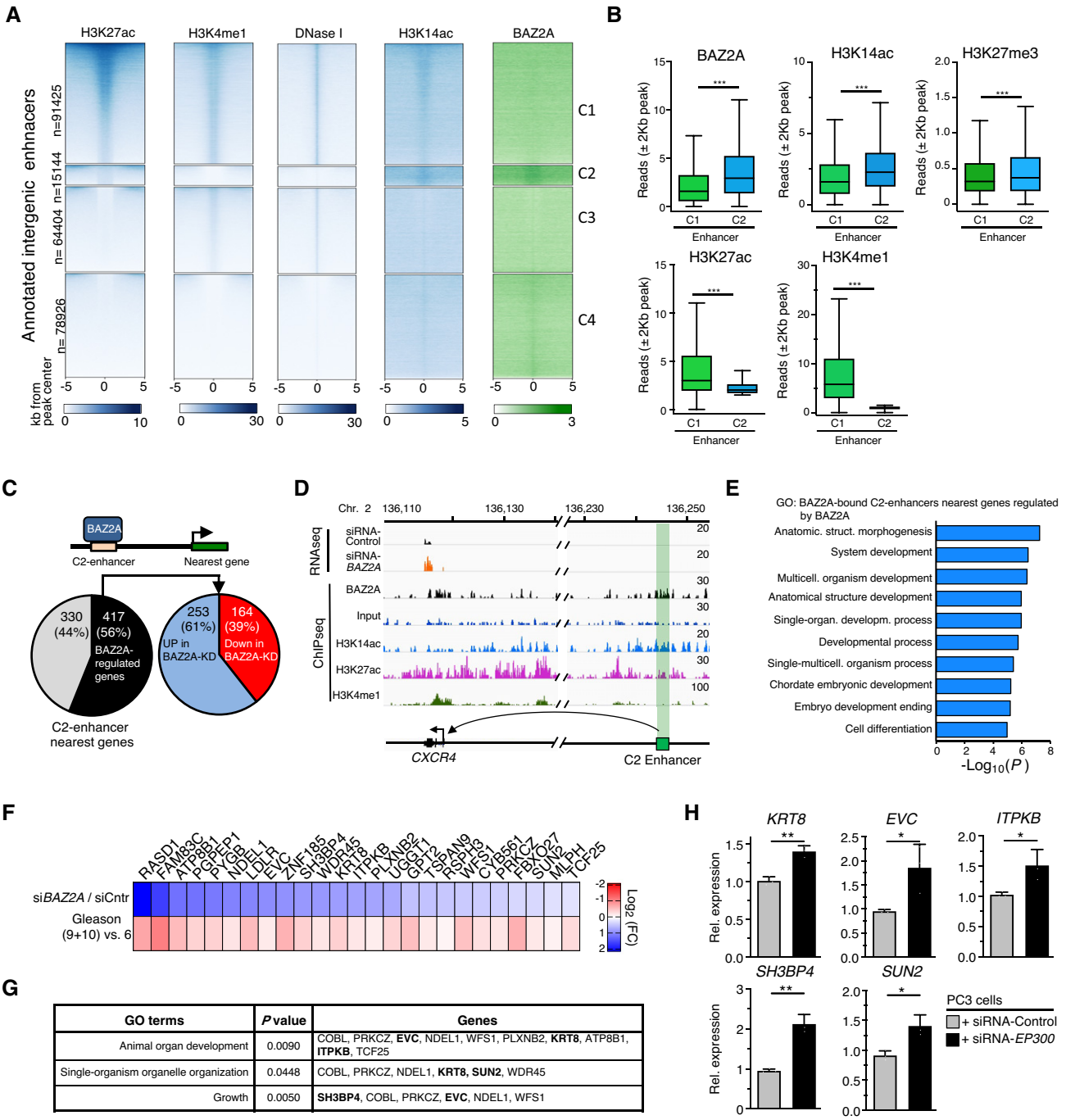

GO terms	*P* value	Genes
Animal organ development	0.0090	COBL, PRKCZ, **EVC**, NDEL1, WFS1, PLXNB2, **KRT8**, ATP8B1, **ITPKB**, TCF25
Single-organism organelle organization	0.0448	COBL, PRKCZ, NDEL1, **KRT8, SUN2**, WDR45
Growth	0.0050	**SH3BP4**, COBL, PRKCZ, **EVC**, NDEL1, WFS1

Figure 3.

small fraction (~1%) of cells that can generate tumorspheres (Li *et al*, 2008; Sheng *et al*, 2013) and become significantly more clonogenic, chemoresistant, and invasive compared with the heterogeneous PC3 cell population (Civenni *et al*, 2013; Portillo-Lara & Alvarez, 2015). Tumorspheres isolated from PC3 cells (PC3-CSCs) could be serially passaged *in vitro,* and when plated in adherent growth conditions, they could differentiate into monolayer cultures morphologically indistinguishable from the original PC3 cells (Fig EV3A). To further characterize the obtained PC3-CSCs, we performed RNAseq analysis and found that 1,906 genes display transcriptional changes ($\log_2$ fold change > 1; $P < 0.05$; 922 upregulated and 984 downregulated in PC3-CSCs vs PC3 cells; Fig 4A, Dataset EV4). GO analysis indicated that genes downregulated in PC3-CSCs were associated with developmental processes (i.e., *HOXA1, HOXA4, SOX7*), reflecting a more dedifferentiated state compared with the parental PC3 cells (Fig 4B and C). Furthermore, gene set enrichment analysis (GSEA) using predefined embryonic stem cell (ESC)-like gene signatures showed that genes upregulated in PC3-CSCs were enriched in adult stem cell signatures (Wong *et al*, 2008) and displayed a transcription profile similar to genes highly

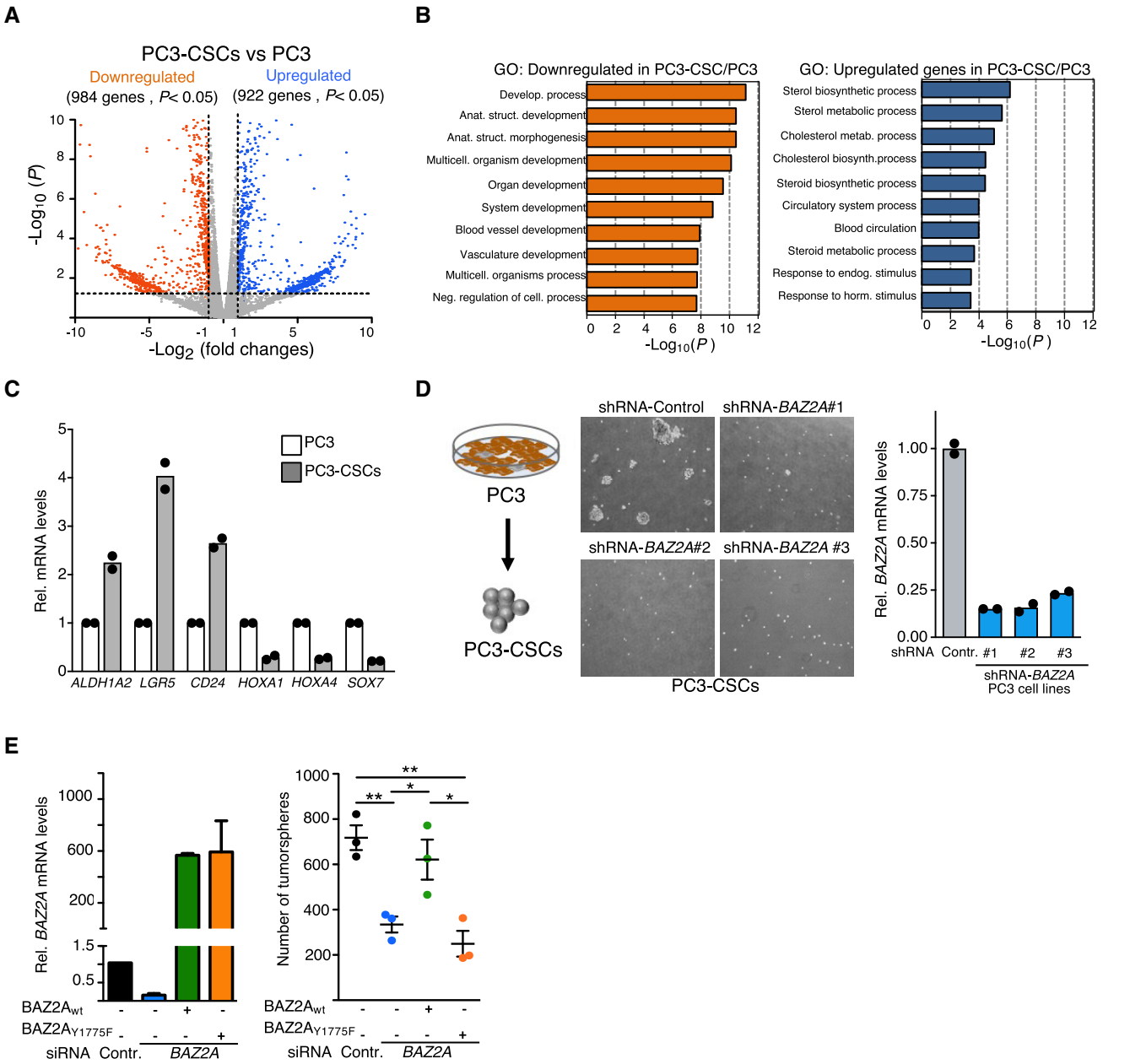

Figure 4. BAZ2A-bromodomain is required for PCa stem cells.

A RNAseq showing differential gene expression between PC3-CSCs and the parental PC3 cells ($P < 0.05$, Log_2 fold change 1).

B Top 10 biological process gene ontology (GO) terms as determined using DAVID 6.8 for genes downregulated and upregulated in PC3-CSCs relative to parental PC3 cells.

C qRT–PCR of genes differentially expressed in PC3-CSCs compared with PC3 cells showing the upregulation of CSC markers (*ALDH1A2*, *LGR5*, *CD24*) *and* downregulation of genes related to developmental processes (*HOXA1*, *HOXA4*, *SOX7*). Data are from two independent experiments. mRNA levels were normalized to *GAPDH*.

D BAZ2A is required for the dedifferentiation of PC3 into PC3-CSCs. Left panel: Representative images from two independent experiments showing the impairment of PC3 cells to form tumorspheres upon stable depletion of BAZ2A. Right panel: *BAZ2A* mRNA levels in three independent PC3 cell lines stably expressing shRNA-*BAZ2A* were measured by qRT–PCR and normalized to *GAPDH* mRNA from 2 independent experiments.

E Left panel: qRT–PCR showing *BAZ2A* mRNA levels in PC3 cells depleted of endogenous *BAZ2A* with siRNA specifically targeting human *BAZ2A* sequences and expressing mouse BAZ2Awt and BAZ2A-BRD mutant ($BAZ2A_{Y1775F}$). Values were normalized to *MRPS7* mRNA. Data are from three independent experiments. Right panel: Quantification of tumorspheres from three independent experiments. Statistical significance (*P*-values) was calculated using two-tailed *t*-test (*< 0.05; **< 0.01). Error bars represent SD.

expressed in human embryonic stem cells compared with differentiated cells (Ben-Porath *et al*, 2008; Wong *et al*, 2008) (Fig EV3B). Importantly, among the upregulated genes we found markers associated with CSCs such as *LGR5*, *CD24, Nestin*, *EpCAM,* and *ALDH1A2* (Raha *et al*, 2014; Cao *et al*, 2017; Li *et al*, 2017) (Figs 4C and EV3C). Taken together, these results indicated that tumorspheres derived from PC3 cells have a gene signature that resemble the molecular signature of a cancer stem cell-like phenotype.

To determine whether BAZ2A is implicated in CSCs, we established three PC3 cell lines stably expressing shRNA against *BAZ2A* sequence (Fig 4D). Remarkably, all shRNA-*BAZ2A* PC3 cell lines were unable to generate PC3-CSCs. Similarly, treatment of PC3 cells with siRNA-*BAZ2A* reduced the number of tumorspheres (Fig 4E). This phenotype could be rescued upon ectopic expression of mouse BAZ2A, which is not targeted by the siRNA-*BAZ2A*. Importantly, the expression of the bromodomain-mutant $mBAZ2A_{Y1775F}$ abrogated the formation of tumorspheres, indicating that a functional BAZ2A-bromodomain is critical for the CSC-like properties of PC3 cells (Fig 4E). Collectively, these results indicate that a functional BAZ2A-bromodomain is required for PC3-CSCs and supported a role of BAZ2A in driving aggressive and poorly differentiated PCas.

Pharmacological inhibition of BAZ2A-bromodomain impairs PCa stem-like cells and the oncogenic transformation mediated by *Pten*-loss

The requirement of a functional BAZ2A-bromodomain for PC3-CSCs prompted us to test the possibility to inhibit BAZ2A-bromodomain for targeting CSCs as a therapeutic strategy. Recently, two chemical probes, GSK2801 and BAZ2-ICR, have been generated for specific targeting of bromodomains of BAZ2A and the closely related BAZ2B (Chen *et al*, 2015; Drouin *et al*, 2015), which display 65% sequence similarity (Tallant *et al*, 2015). Both compounds are highly specific for BAZ2A- and BAZ2B-bromodomains and show half-maximal inhibitory concentration (IC50) in the nanomolar range (Chen *et al*, 2015; Drouin *et al*, 2015). To determine whether BAZ2-ICR or GSK2801 destabilizes BAZ2A-bromodomain interaction with histones, we incubated recombinant BAZ2A-bromodomain with both compounds and measured BAZ2A-bromodomain binding to modified histones with the histone peptide array (Figs 5A and EV4A). Both BAZ2-ICR and GSK2801 abolished the interaction of BAZ2A-bromodomain with histones, although GSK2801 inhibition was weaker than BAZ2-ICR.

Next, we tested the possibility to impair BAZ2A function in PCa cells through pharmacological targeting of BAZ2A-bromodomain. Treatment of PC3 cells with BAZ2-ICR upregulates the expression of several BAZ2A-regulated genes such as *AOX1*, *DDB1*, *SH3BP4*, and *EVC* without affecting BAZ2A and H3K14ac levels (Fig EV4B and C). Previous results showed that BAZ2A depletion in several metastatic PCa cells, including PC3 cells, impairs cell proliferation (Fig 5B) (Gu *et al*, 2015). Indeed, all our attempts to isolate BAZ2A-KO PC3 cell lines through CRIPS/Cas9 failed, indicating the requirement of BAZ2A expression in metastatic PCa cells. Surprisingly, treatment of PC3 cells with BAZ2-ICR or GSK2801 at concentrations up to 50 μM did not affect cell proliferation (Figs 5C and EV4D), suggesting that BAZ2A-bromodomain is not functionally relevant in the proliferation of the heterogeneous PC3 cell population. In contrast, treatment with BAZ2-ICR or GSK2801 from the beginning of the culture of PC3 cells in low adhesion plate drastically reduced the number of tumorspheres (EC_{50} 0.83 μM; Fig 5D and E), indicating that pharmacological targeting of BAZ2A-bromodomain impairs PC3-CSCs. The different effects of BAZ2A inhibitors did not depend on different BAZ2A expression levels since BAZ2A is expressed at similar levels in both PC3 and tumorspheres (Fig EV4E). The abrogation of tumorsphere formation upon treatment with BAZ2A-bromodomain inhibitors could also be observed in another metastatic PCa cell line, DU-145 (Fig 5F). These results are consistent with the data showing the tumorspheres require a functional BAZ2A-bromodomain (Fig 4E). Since BAZ2-ICR or GSK2801 can also target BAZ2B-bromodomain (Chen *et al*, 2015; Drouin *et al*, 2015), we tested the contribution of BAZ2B in PC3-CSCs by transfecting PC3 cells with siRNA directed against *BAZ2B* that is similarly expressed in both PC3 and PC3-CSCs (Fig 4E and F). We found no detectable defects compared with control cells, indicating that pharmacological targeting of BAZ2A-bromodomain has a major function in PCa cells with CSC-like state.

Next, we analyzed the role of BAZ2A-bromodomain in PCa initiation using mouse prostate organoids to model PCa driven by the loss of *Pten*, one of the most commonly lost tumor suppressor gene in PCa (Yoshimoto *et al*, 2006; Berger *et al*, 2011; Phin *et al*, 2013; Karthaus *et al*, 2014; Cancer Genome Atlas Research Network, 2015) (Fig 6). PTEN was also shown to have a pivotal role in CSCs by regulating pathways critical for stem cell maintenance, homeostasis, self-renewal, and migration (Wang *et al*, 2006; Mulholland *et al*, 2009; Luongo *et al*, 2019). Furthermore, recent results showed that BAZ2A is required for the initiation of PCa driven by *PTEN*-loss (Pietrzak *et al*, 2020). Downregulation of *Pten* was achieved by infection of prostate organoids with lentivirus encoding shRNA-*Pten*, which allowed 80% global reduction in *Pten* levels (Fig EV5A). Consistent with previous reports (Karthaus *et al*, 2014; Pietrzak *et al*, 2020), compared to control organoids, shRNA-*Pten* organoids displayed altered morphology as evident by the solid and compact structure and elevated expression of nuclear proliferation marker Ki67, without altering the number of organoids (Fig 6A–E). Remarkably, treatment with BAZ2A-bromodomain inhibitors BAZ2-ICR or GSK2801 followed by transduction with shRNA-control or shRNA-*Pten* impaired *Pten*-loss mediated transformed phenotype as evident by the translucent phenotype, the intact bilayer structure, and low Ki67 signal whereas EZH2 inhibitor GSK126 did not show any significant effect (Fig 6A–D). These results are consistent with previous data showing that BAZ2A is required for the initiation of PCa driven by *Pten*-loss (Pietrzak *et al*, 2020) and highlighted an important role of BAZ2A-bromodomain in this process. Collectively, these data indicate that pharmacological targeting of BAZ2A-BRD abolishes PCa cells with CSC-like state and the oncogenic transformation mediated by *Pten*-loss.

Discussion

Previous work showed that BAZ2A, a component of the chromatin remodeling complex NoRC, is implicated in aggressive PCa (Gu *et al*, 2015; Pietrzak *et al*, 2020). In this study, we showed that BAZ2A-bromodomain is required for PCa cells with a cancer stem-like state and the initiation of PCa driven by *PTEN*-loss. We showed that BAZ2A-bromodomain is an epigenetic reader of H3K14ac and is required for the association of BAZ2A with a class of inactive

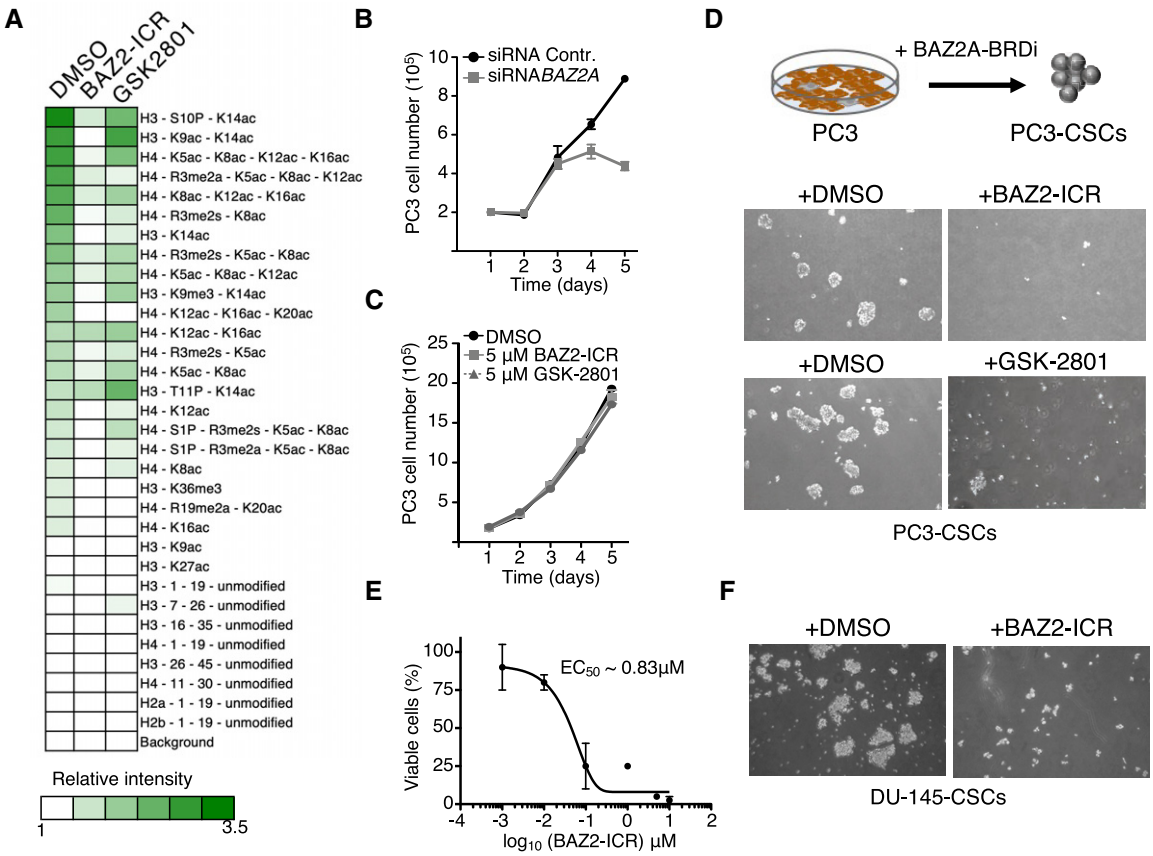

Figure 5. Pharmacological targeting of BAZ2A-bromodomain impairs the transition of PCa cells into a dedifferentiated, cancer stem-like state.

A Heatmaps showing the relative BAZ2A-BRD binding intensity at modified histone peptides upon incubation with BAZ2A-BRDi BAZ2-ICR or GSK2801 displayed in Fig EV4A. Binding intensity was calculated as average of fold change from peptides signal over background controls of two different arrays.

B Cell proliferation curves of PC3 cells treated with siRNA-*BAZ2A*. Error bars represent the standard deviation from three independent experiments.

C Cell proliferation curves of PC3 cells treated with 5 μM BAZ2-ICR and GSK2801. Error bars represent the standard deviation from three independent experiments.

D Representative images of tumorspheres generated from PC3 cells treated with BAZ2-ICR (1 μM) or GSK2801 (1 μM).

E Half-maximal effective concentration (EC50) of BAZ2-ICR. Measurements were performed 5 days after treatment of PC3 cells and initiation of tumorspheres using the indicated BAZ2-ICR concentration. The amount of tumorspheres was assessed by measurement of cell viability. Error bars represent SD. Values are from three independent experiments.

F Representative images showing tumorspheres derived from the metastatic PCa cell line DU-145 treated with DMSO or BAZ2-ICR (1 μM) inhibitor for 5 days.

enhancers that are marked by H3K14ac. We showed that the expression of a large fraction of genes in the nearest linear genomic proximity to these BAZ2A-bound enhancers depends on BAZ2A. These genes are implicated in developmental and differentiation pathways, which are usually altered in aggressive and dedifferentiated PCa. The expression analysis of a set of genes that are repressed by BAZ2A and frequently silenced in advanced and poorly differentiated tumors relative to indolent tumors showed the requirement of EP300, one of the writers of H3K14ac. The link of H3K14ac with gene silencing is also consistent with previous studies showing that the transcription regulator ZMYND8, the tumor suppressor PBRM1, and H3K9 methyltransferase SETDB1 can recognize H3K14ac and repress gene transcription (Li *et al*, 2016; Jurkowska *et al*, 2017; Liao *et al*, 2019). The interaction of BAZ2A-bromodomain with H3K14ac is also of particular interest since H3K14ac was found to be the most prominent histone modification in regulating SNF2H/ISWI nucleosome remodeling and activating only the NoRC complex (Dann *et al*, 2017). Thus, it is possible that H3K14ac is not only acting for the recruitment of BAZ2A to chromatin but also for the remodeling of nucleosomes that might play a role in the regulation of gene expression. A BAZ2A-mediated remodeling at nucleosomes marked with H3K14ac might therefore be part of the mechanisms to silence gene expression and future studies will address this point.

Cancer stem cells represent a subpopulation within tumors that has an enhanced capacity for therapeutic resistance and thought be implicated in relapse of many tumors' types, including PCa (Flemming, 2015; Mayer *et al*, 2015; Zhang *et al*, 2017). Further, cancer cells can transition between stem and differentiated states in response to therapeutic insults or other stimuli within the microenvironment (Plaks *et al*, 2015; Rich, 2016). Thus, efficient targeting of cancer stem cells in cancer treatment is critical for developing effective therapeutics. In this work, we used an established method to measure the ability of PCa cells to form tumorspheres (Rajasekhar *et al*, 2011; Portillo-Lara & Alvarez, 2015). We showed that

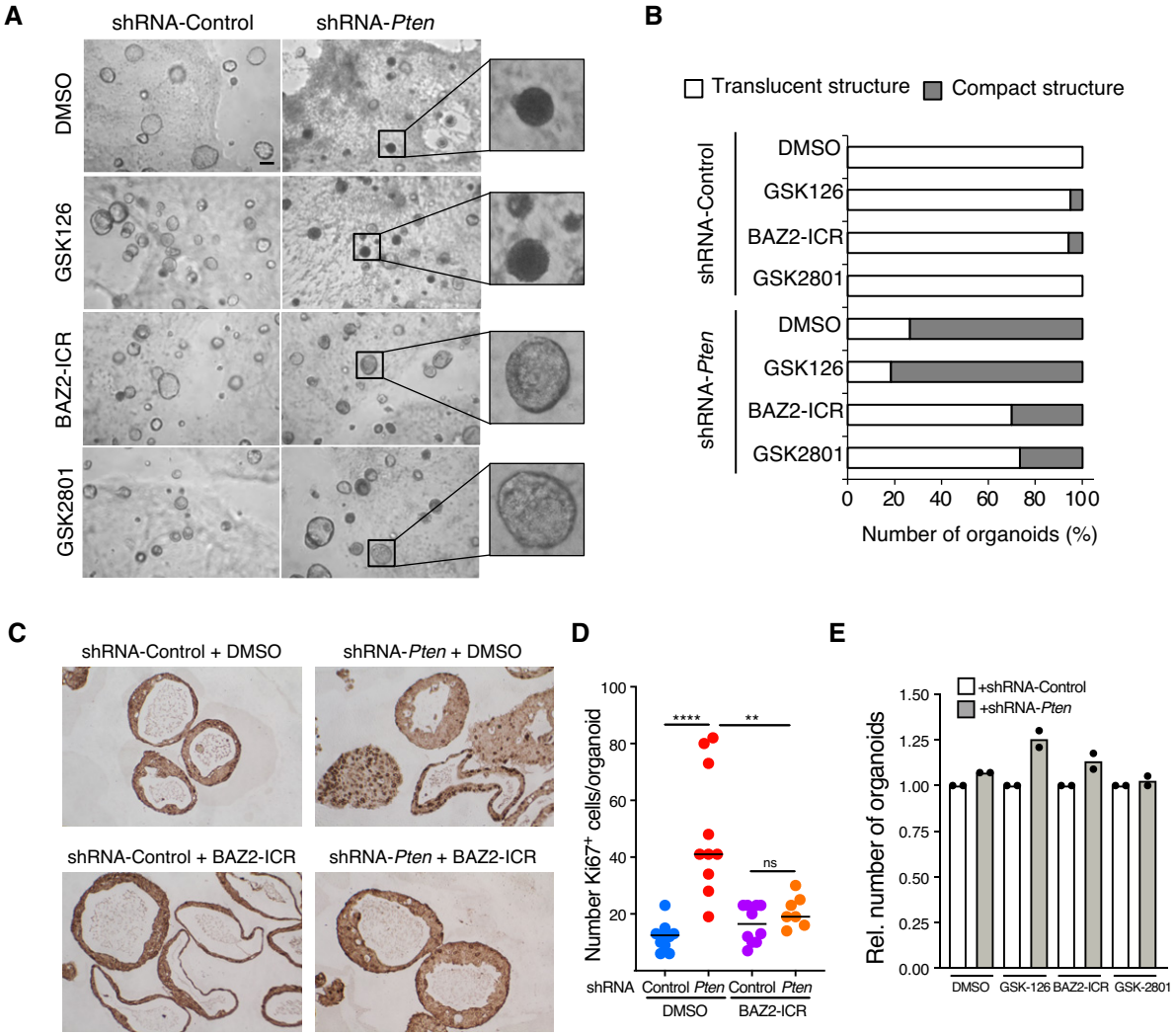

Figure 6. Pharmacological targeting of BAZ2A-bromodomain impairs the initiation of PCa driven by *Pten* loss in a model of PCa organoids.

A Representative brightfield images of organoids derived from mouse prostate cells treated with DMSO, BAZ2-ICR (5 μM), GSK2801 (5 μM), or GSK126 (5 μM) inhibitors followed by transduction with shRNA-control or shRNA-*Pten*.

B Quantification of shRNA-control and shRNA-*Pten* organoid morphology upon treatment with DMSO, EZH2 (GSK126), and BAZ2A-BRD inhibitors (BAZ2-ICR and GSK2801).

C Representative images of Ki67-immunostained mouse prostate organoid sections expressing shRNA-control and shRNA-*Pten* and treated with DMSO or BAZ2-ICR (5 μM).

D Quantification of $Ki67^+$ cells in mouse prostate organoids shown in (C). **< 0.01, ****$P < 0.0001$, two-tailed Student's *t*-test; ns, not significant. The median values are represented by a line.

E Quantification of mouse prostate organoids per field expressing shRNA-control and shRNA-*Pten* and treated with DMSO, GSK126 (5 μM), BAZ2-ICR (5 μM), or GSK2801 (5 μM). Values were normalized to shRNA-control samples. Average values of two independent experiments.

BAZ2A-bromodomain is required for PCa cells with cancer stem-like properties, suggesting that targeting BAZ2A with BAZ2A-bromodomain inhibitors in tumors should be beneficial in impairing cancer cells with a stem-like state, thereby decreasing tumor relapse potential.

Current therapeutic approaches for PCa remain insufficient for some patients with progressive disease. Targeting AR axis can manage PCa relapses only for a limited time period since PCas become unresponsive and progress to a castrate-resistant form with limited treatment options (Linder *et al*, 2018). The development of PCa stem cell-specific anticancer drugs constitutes an attempt to innovate the treatment of PCa (Leão *et al*, 2017). Previous results showed that AR-signaling-competent human CRPC cell lines are preferentially sensitive to BET inhibitors JQ1 (Asangani *et al*, 2014). However, inhibition of BET-BRD does not have an effect in AR-independent cell lines such as PC3 cells (Asangani *et al*, 2014). Our study demonstrated that BAZ2A-bromodomain function can be pharmacologically targeted through BAZ2A-BRD inhibitors in CRPC cells and proposed that inhibition of BAZ2A-bromodomain can be a potential strategy to use against cancer stem cells in PCa.

Materials and Methods

Culture of PC3 and PCa spheres

All the indicated cell lines were purchased from the American Type Culture Collection. PC3 cells were cultured in RPMI 1640 medium and Ham's F12 medium (1:1; Gibco) containing 10% FBS (Gibco) and 1% penicillin–streptomycin (Gibco). DU-145 were cultured in RPMI 1640 medium containing 10% FBS and 1% penicillin–streptomycin. PCa spheres were cultured in serum-free DMEM/F12 medium (1:1, Gibco) supplemented with 20 ng/ml of basic human FGF (Sigma), 20 ng/ml of EGF (Sigma), 3 μg/ml of Insulin (Sigma), and 1× B27 (Gibco). 1×10^4 cells were seeded into low adhesion petri dishes (Greiner) and cultured for 6–8 days. About 20% of media was changed every 2 days. All cells were regularly tested for mycoplasma contamination. PC3 cells were treated with 1 μM of BAZ2A-BRD inhibitors BAZ2-ICR (SML1276, Sigma) and GSK2801 (SML0768, Sigma), EZH2 inhibitor GSK126 (S7061-5MG, Lubio), BET inhibitors JQ1 (SML1524, Sigma), or DMSO as control. Fresh medium supplemented with the drugs was added every 2 days. PCa spheres were culture for 6 days. Cells were collected and transferred to a 24-well plate to image and quantify the number of PCa spheres upon drug treatments.

Culture of prostate organoids

Isolation of prostate epithelial cells was performed as previously described (Karthaus *et al*, 2014; Pietrzak *et al*, 2020). Murine prostate lobes were isolated from 10- to 11-week-old mice under dissection microscope, macerated with blade, and transferred into tube containing 1.5 ml solution of collagenase/hyaluronidase (Stem Cell Technologies) in ADMEM/F12 (Gibco Life Technologies) containing 100 μg/ml Primocin (InvivoGen). Subsequently, prostate tissue was incubated at 37°C rocking for 2 h. After collagenase digestion, samples were centrifuged at 350 *g* for 5 min, supernatant was discarded and cell pellet was washed with HBSS (Life Technologies). To dissociate prostate tissue into single cells, cell pellet was mixed with 5 ml TrypLE (Gibco Life Technologies) with the addition of 10 μM ROCK inhibitor Y-27632 (STEMCELL Technologies) and incubated for 15 min at 37°C followed by pipetting up and down several times. Subsequently, HBSS + 2% FBS (Gibco; equal to 2× volume of TrypLE) was added to dissolve TrypLe and quench the reaction. Trypsinized prostate tissue was centrifuged at 350 *g* for 5 min, supernatant was discarded, and the pellet was washed with HBSS and centrifuged again. 1 ml of pre-warmed Dispase (STEMCELL Technologies)/DNaseI (STEMCELL Technologies) solution was added, and samples were vigorously and continuously pipetted up and down until solution was homogenously translucent with no visible tissue fragments. Samples were centrifuged to remove Dispase solution, and cell pellet was washed with ADMEM/F12 containing 2% FBS (equal to 5× volume of Dispase). To obtain single cells, suspension was filtered through a 40-um cell strainer and centrifuged, and then, supernatant was removed. Cells were resuspended in ADMEM/F12 + 2% FBS, and viable cells were counted using hemocytometer and trypan blue.

Generation of organoids was performed as previously described (Pietrzak *et al*, 2020). Prostate cells were resuspended in cold ADMEM/F12 5+ medium at density 5,000 cells per 40 μl for total organoid culture. Cell suspension was mixed with 60 μl of pre-thawed growth factor reduced Matrigel (Corning) and plated in a form of drop into the middle of a well from 24-well plate (TPP). Organoids were cultured in 500 μl of ADMEM/F12 supplemented with B27 (Gibco Life Technologies), GlutaMax (Gibco Life Technologies), 10 mM HEPES (Gibco Life Technologies), 2% FBS, 100 μg/ml Primocin (ADMEM/F12 5+ medium), and contained following growth factors and components: mEGF (Gibco Life Technologies), TGF-β/Alk inhibitor A83-01 (Tocris), dihydrotestosterone (DHT; Sigma-Aldrich) with the addition of 10 μM ROCK inhibitor Y-27632 for the first week after seeding (organoid culture complete medium). Medium was changed every 2–4 days by aspiration of the old one and addition of fresh 500 μl of culture organoid medium. Sequences encoding control shRNA (CACAAGCTGGAGTACAACTAC) and shRNA targeting *Pten* (CGA CTTAGACTTGACCTATAT) were cloned into lentiviral vectors. Lentiviral supernatants were concentrated 100 times using Lenti-X Concentrator (Clontech) according to manufacturer's protocol. 40 μl of concentrated virus was mixed with 100.000 cells suspended in transduction medium (ADMEM/F12, B27 GlutaMax, 10 mM HEPES, 100 μg/ml Primocin, 2 μg/ml Polybrene (Sigma-Aldrich), 10 μM ROCK inhibitor). Cells were incubated with virus for 20 min at RT, centrifuged for 40 min at 800 *g* at RT, and placed in incubator for 3.5 h to recover. Cells were plated in Matrigel at 5,000 cells/well density, and after 3 days postseeding, 1 μg/ml puromycin (Gibco) was applied to select organoids stably expressing shRNA-control or shRNA-*Pten*.

Organoids were cultured for 22 days in the presence of 5 μM of BAZ2A inhibitors BAZ2-ICR (SML1276, Sigma), GSK2801 (SML0768, Sigma), EZH2 inhibitor GSK126 (S7061-5MG, Lubio), BET inhibitors JQ1 (SML1524, Sigma) or DMSO as control. Medium was replaced every 2 days with 500 μl of fresh medium supplemented with inhibitors.

Establishment of FLAG-HA-BAZ2A PC3 cell line

In order to introduce the FLAG-HA tag in *BAZ2A* locus, a donor plasmid was synthetized by IDT containing the genomic sequence of the FLAG-HA tag flanked by ± 1 KB homology arm to *BAZ2A* locus. Generation of stable cell was achieved by Alt-R™ CRISPR-Cas9 system from IDT as per manufacturer protocol. A crRNA guide sequence (CCTTCTCTCCCAGTTCTCGG) was chosen to target the *BAZ2A* locus on exon 2 three base pairs upstream of the ATG start codon. Equimolar concentrations of RNA oligos synthetized by IDT (sgRNA and transactivating crRNA) were mixed in Nuclease-Free Duplex Buffer (IDT) to a final concentration of 1 μM and were hybridized by heating the mix at 95°C 5 min and cooling it down to RT. 1 μl of hybridized RNA oligos was incubated with 1 μM of Cas9 protein (IDT) in Opti-MEM I Reduced-Serum Medium (Gibco) and incubated at RT for 15 min to form a ribonucleoprotein (RNP) complex. RNP complex was transfected for 48 h with Lipofectamine RNAiMax (Invitrogen) to 4×10^4 PC3 previously transfected with donor plasmid carrying the desired inclusion sequence. Single cell clones were isolated and grew until colonies were big enough to be genotyped. To assess the integration of FLAG-HA tag in *BAZ2A* locus, two oligos were designed to amplify a genomic region that spans the FLAG-HA tag and a region 150 bp outside of the left homology arm that is not encoded in the donor plasmid. Genotyping

of clones was performed using primers amplifying the region that spans the insertion site of FLAG-HA tag within *BAZ2A* locus, where a product of 230 bp represents the wild-type allele and a product of 300 bp indicates the integration of the FLAG-HA tag (primers are listed in Table 1).

Expression and purification of recombinant proteins

Sequence corresponding to *BAZ2A*-bromodomain (residues 1,797–1,899) was codon optimized for robust expression in E. coli and cloned into pGex4T-1. *BAZ2A*-bromodomain mutants (Y1830F, N1873L) were achieved by single point mutation PCR and sequenced to ensure accuracy of the point mutations (primers are listed in Table 1). The expression of recombinant proteins was achieved by transforming E. coli competent BL21 bacteria with 600ng of plasmids expressing BAZ2A-bromodomain. Bacteria were grown at 37°C in Terrific Broth (24 g/l yeast extract, 20 g/l tryptone, 4 ml/l glycerol, 0.017 M KH_2PO_4, and 0.072 M K_2HPO_4) until reached an OD of 0.6–0.7 at 600 nm of absorbance. Induction of the expression of recombinant proteins was done at 16°C overnight by supplementing the inoculated culture with 0.5 mM IPTG. Bacteria were harvested by centrifugation, and pellet was resuspended in 4× (w/v) lysis buffer (20 mM Tris pH7.5, 300 mM NaCl, 1 mM DTT, 20% glycerol, 1 mM PMSF) and sonicated 3× 30 s on/off. After sonication, lysates were treated with DNase I (50 U) and RNase-A (50 μg) 30 min at 4°C with constant rotation. Lysates were then spun down, and supernatant was collected and filtered (0.22 μM). GST-fusion proteins were purified using Glutathione-Sepharose 4B beads (GE Healthcare). Purified proteins were eluted with 20 mM Glutathione and dialyzed overnight (20 mM Tris pH 7.5, 100 mM

Table 1. List of primers used in this study.

Gene	Forward (5′–3′)	Reverse (5′–3′)
Cloning		
hBAZ2A-BRD_mutant (Y1830F)	ggtcagcggctTtcgccgtatcatcaaaaacc	ggtttttgatgatacggcgaAagccgctgacc
hBAZ2A-BRD_mutant (N1873L)	gtcagaccttcCTtgaagatgacagc	gctgtcatcttcaAGgaaggtctgac
mBAZ2A-BRD_mutant (Y1775F)	ggtgagtggaTTCcgacgtgtcatcaagaacc	ggttcttgatgacacgtcgGAAtccactcacc
Genotyping		
BAZ2A_FLAG-HA-tag_insertion	CTCAGGTGAGCCACCGTAC	TCGAGCTTGTCGTCATCGTC
BAZ2A_FLAG-HA-tag_genotyping	TGCTCAGGCTAGAGGCATATT	CAGGGGGAAGGCCAGTAAAG
ChIP_qPCR		
AOX1	GTTCGTCCCATCCTTTCGT	CCTGAAAACGCAGCCTTTAG
GAPDH	CGGGATTGTCTGCCCTAATTAT	GCACGGAAGGTCACGATGT
EVX1	TACACAGCATCTGGGGAGTG	GTGTGCTGGGTTAAGGGAGA
qRT–PCR		
ALDH1A2	AGCTGGGACTGTTTGGATCA	ACTCCCGCAAGCCAAATTCT
LGR5	AGCATTCACTGGCCTTTACAGT	CATCCAGACGCAGGGATTGAA
CD24	CTGCTGGCACTGCTCCTAC	GGCATTAGTTGGATTTGGGGC
HOXA1	CACGCCAGCCACCAAGA	ACTTTCCCTGTTTTGGGAGGG
HOXA4	ATGTCAGCGCCGTTAACCC	CCTTCTCCAGCTCCAAGACC
SOX7	TTCATGGTTTGGGCCAAGGA	CCACGACTTTCCCAGCATCT
MRPS7	AGCCTATGATTGGGCTGGTA	CGGCACTCAGTGATCATCC
RPS3A	AATCATGACCCGAGAGGTGC	TCCAATGCTGTCTGGAATCAATTT
BAZ2A	AAGATGTGTGGCTACAATGG	TCTGCACCCATCAGCTCCG
KRT8	TAAGGATGCCAACGCCAAGT	AGACTCCAGCCGGCTCTC
EVC	ACGCGACACCAGAAAGACG	TATTGCTGTTGGAAGGCGGC
ITPKB	TTCAAGTGCCACGAGGTCAT	GGTTATTGAGCCCCGAGAGG
SH3BP4	GAGCTTGTGATGGCCCTACT	GTCCATCTGCTGCTTGGAGA
SUN2	CGAGTCATCCTCCAGCCAGA	GCTGCAGGTCTTCGTCAAAC
EP300	CCTGGGTCCTATGCCAACAG	TGGCTTGGACGAGTTTGTGA
AOX1	CGACAAGCCCAGCGACAGG	GTGGCTGGACCAACGCCTCC
MAN2B2	CTGCAGATCCTGAGCATCCC	AGCACAGCCTCCAGATTCAC
DMPK	GCCTTTTGTGGGCTACTCCT	GCCACTTCAGCTGTTTCATCC
DDB1	TCAACGGCATGATAGGGCTG	CGCTCGGTGTGAAAGGATCT

NaCl, 2 mM EDTA, 20% Glycerol). Purity of eluted proteins was assessed by SDS–PAGE.

Histone peptide arrays

MODified Histone Peptide Arrays were acquired from Active Motif. Briefly, arrays were blocked for 4 h with Odyssey® Blocking Buffer diluted in PBS (1:1). Binding of recombinant proteins to histone peptide array was done by diluting 10 nM of recombinant GST or GST-BAZ2A proteins in 3ml of HEMG buffer (25 mM HEPES pH 7.6, 12.5 mM $MgCl_2$, 0.5 m EDTA, 1 mM DTT, 0.2 mM PMSF, 10% glycerol) and incubated overnight at 4°C. Pharmacological inhibition of GST-BAZ2A-BRD was achieved by incubating recombinant proteins with 50 nM of BAZ2-ICR or GSK2801 overnight in HEMG buffer. Detection of binding was determined by 2-h incubation (room temperature) with anti-GST (SC-459, 1:1,000 in Odyssey® Blocking Buffer), followed by 1-h incubation with goat anti-Rabbit (IRDye® 800CW, 1:10,000 in Odyssey® Blocking Buffer). Between incubation periods, histone peptide arrays were washed 3X in PBST to reduce background levels. Arrays were scanned on Odyssey Infrared Imaging System. Active Motif's Array Analyzer software was used to identify peptides bound by recombinant proteins, and intensity of binding was measured as fold changes over background level.

Plasmid and siRNA transfections

cDNA corresponding to mouse *BAZ2A* wild type was cloned into AASV1 donor vector (DC-DON-SH01, GeneCopoeia). Site-directed mutagenesis was performed to create *BAZ2A*-bromodomain mutant (Y1775F), and sequencing of plasmid was performed to ensure fidelity of sequences. 1×10^6 of PC3 cells were transfected for 48 h with 8 μg of plasmids with X-tremeGENE HP DNA Transfection Reagent (Roche). siRNA against *BAZ2A* (Cat. # SI00102389) and siRNA-control (Cat. # 1027281) was obtained from Qiagen. EP300 siRNA (Cat. # J-003486-11-0002) and BAZ2B siRNA (Cat. # D-020487-02-0005) were obtained from Dharmacon. Transfections of siRNA were performed with Lipofectamine RNAiMax (Invitrogen) in Opti-MEM Reduced-Serum Medium (Gibco).

Chromatin immunoprecipitation

ChIP experiments were performed as previously described (Leone *et al*, 2017). Briefly, 1% formaldehyde was added to cultured cells to cross-link proteins to DNA. Isolated nuclei were then lysed (50 mM Tris–HCl pH 8.1, 10 mM EDTA and 1% SDS) and sonicated using a Bioruptor ultrasonic cell disruptor (Diagenode) to shear genomic DNA to an average fragment size of 200 bp. 20 μg of chromatin was diluted tenfold with ChIP buffer (16.7 mM Tris–HCl pH 8.1, 167 mM NaCl, 1.2 mM EDTA, 0.01% SDS, and 1.1% Triton X-100) and precleared for 2 h with 10 μl of packed Sepharose beads for at least 2 h at 4°C. Immunoprecipitation was done overnight with the indicated antibodies. Pulldowns were done with Dynabeads protein-A (or -G, Millipore) for 4 h at 4°C. For HA-BAZ2A ChIPs, preclearing and pulldowns were done with beads block with BSA (50 μg) and ytRNA (50 μg), per 400 μl of Dynabeads protein-A. After washing, elution, and reversion of cross-links, eluates were treated with RNAse A (1 μg). DNA was purified with phenol–chloroform, ethanol precipitated, and quantified by quantitative PCR. Primer sequences and antibodies are listed in Tables 1 and 2.

ChIPseq analysis

The quantity and quality of the isolated DNA was determined with a Qubit® (1.0) Fluorometer (Life Technologies, California, USA) and a Bioanalyzer 2100 (Agilent, Waldbronn, Germany). The NEBNext® Ultra™ II DNA Library Prep Kit from NEB (New England Biolabs, Ipswich, MA) was used in the succeeding steps. ChIP samples (1 ng) were end-repaired and adenylated. Adapters containing the index for multiplexing were ligated to the fragmented DNA samples. Fragments containing adapters on both ends were enriched by PCR. The quality and quantity of the enriched libraries were measured using Qubit® (1.0) Fluorometer and the TapeStation (Agilent, Waldbronn, Germany). The product is a smear with an average fragment size of approximately 300 bp. The libraries were normalized to 10 nM in Tris-Cl 10 mM, pH8.5 with 0.1% Tween 20. The TruSeq SR Cluster Kit v4-cBot-HS (Illumina, Inc, California, USA) was used for cluster generation using 8 pM of pooled normalized libraries on the cBOT. Sequencing was performed on the Illumina HiSeq 2500 single end 125 bp using the TruSeq SBS Kit v4-HS (Illumina, Inc, California, USA). Obtained ChIPseq reads from Illumina HiSeq 2500 were aligned to the human hg38 reference genome using Bowtie 2 (version 2.2.5). Read counts were computed and normalized using "bamCoverage" from deepTools (version 2.0.1 (Ramirez *et al*, 2014)) using a bin size of 50 bp. deepTools was used to generate all heat maps, Pearson correlation plots. Peaks from ChIPseq experiments were defined using MACS2 (version 2.1.0 (Zhang *et al*, 2008)) comparing ChIP signal against input. For all histone modifications, default settings were used. BAZ2A peaks were determined using a *P*-value cutoff as < 0.01. Data sets from H3K4me1 (GSM2534170) and DNAse I (GSM2400265) were obtained from ENCODE (ENCODE Project Consortium, 2012) (see also Table 3). Integrative Genome Viewer (IGV, version 2.3.92 (Robinson *et al*, 2011) was used to visualize and

Table 2. List of antibodies used in this study.

	Company	Cat. number
Ab used for ChIP		
H3K27me3	Active Motif	39155
H3K4me3	Merck	07-473
H3K27ac	Abcam	ab4729
H3K14ac	Active Motif	61433
HA	Abcam	ab9110
Ab used for immunohistochemistry		
Anti-Ki67	Abcam	ab15580

Table 3. List of datasets used in this study.

H3K4me1	https://www.ncbi.nlm.nih.gov/geo/query/acc.cgi?acc=GSE96243	ENCODE Project Consortium (2012)
DNase I	https://www.ncbi.nlm.nih.gov/geo/query/acc.cgi?acc=GSE90286	ENCODE Project Consortium (2012)

extract representative ChIPseq tracks. Genomic annotation of ChIPseq peaks was done with ChIPseeker (Yu *et al*, 2015), and promoter regions were defined as ± 5 Kb from TSS. Analysis of overlapping genomic regions was done with bedtools (version 2.27.1 (Quinlan & Hall, 2010)). Enhancer coordinates were obtained from GeneHancer V4.4 (Plaschkes *et al*, 2017), and the read coverage ± 1 Kb from the center of peak was obtained using "computeMatrix" from deepTools with a bin size of 50 bp. Mean read coverage was then used to classify the regions based on the presence or absence of H3K27ac and H3K4me1.

RNA extraction, reverse transcription, and quantitative PCR

RNA was purified with TRIzol reagent (Life Technologies). 1 μg total RNA was primed with random hexamers and reverse-transcribed into cDNA using MultiScribe™ Reverse Transcriptase (Life Technologies). Amplification of samples without reverse transcriptase assured the absence of genomic or plasmid DNA. The relative transcription levels were determined by normalization to *GAPDH* mRNA levels. qRT–PCR was performed with KAPA SYBR® FAST (Sigma) on Rotor-Gene RG-3000 A (Corbett Research). Primer sequences are listed in Table 1.

RNAseq and data analysis

Total RNA from two independent samples form PC3 cells and PCa cells, and from three independent experiments on PC3 cells treated with siRNA control or siRNA-*BAZ2A*, was purified with TRIzol reagent (Life Technologies) as stated above. DNA contaminants were removed by treating RNA with 2 U Turbo-DNaseI (Invitrogen) for 1 h at 37°C, and the RNA samples were re-purified using TRIzol. The quality of the isolated RNA was determined by Bioanalyzer 2100 (Agilent, Waldbronn, Germany). Only those samples with a 260 nm/280 nm ratio between 1.8 and 2.1 and a 28S/18S ratio within 1.5–2 were further processed. The TruSeq RNA Sample Prep Kit v2 (Illumina, Inc, California, USA) was used in the succeeding steps. Briefly, total RNA samples (100–1,000 ng) were poly A enriched and then reverse-transcribed into double-stranded cDNA. The cDNA samples were fragmented, end-repaired, and polyadenylated before ligation of TruSeq adapters containing the index for multiplexing fragments containing TruSeq adapters on both ends were selectively enriched with PCR. The quality and quantity of the enriched libraries were validated using Qubit® (1.0) Fluorometer and the Caliper GX LabChip® GX (Caliper Life Sciences, Inc., USA). The product is a smear with an average fragment size of approximately 260bp. The libraries were normalized to 10 nM in Tris-Cl 10 mM, pH 8.5 with 0.1% Tween 20. The TruSeq SR Cluster Kit HS4000 (Illumina, Inc, California, USA) was used for cluster generation using 10 pM of pooled normalized libraries on the cBOT. Sequencing was performed on the Illumina HiSeq 2500 single end 100 bp using the TruSeq SBS Kit HS2500 (Illumina, Inc, California, USA). Reads were aligned to the reference genome (hg38) with Subread (i.e., subjunc, version 1.4.6-p4; (Liao *et al*, 2013)) allowing up to 16 alignments per read (options: –trim5 10 –trim3 15 -n 20 -m 5 -B 16 -H –allJunctions). Count tables were generated with Rcount (Schmid & Grossniklaus, 2015) with an allocation distance of 10 bp for calculating the weights of the reads with multiple alignments, considering the strand information, and a minimal number of 5 hits. Variation in gene expression was analyzed with a general linear model in R with the package edgeR (version 3.12.0; (Robinson & Oshlack, 2010)) according to a crossed factorial design with two explanatory factors (i) siRNA against *BAZ2A* and a mock sequence and (ii) expression pattern of PCa spheres vs PC3 cells. Genes differentially expressed between specific conditions were identified with linear contrasts using trended dispersion estimates and Benjamini–Hochberg multiple testing corrections. Genes with a *P*-value below 0.05 and a minimal fold change of 1.5 or 2 were considered to be differentially expressed. These thresholds have previously been used characterizing chromatin remodeler functions (de Dieuleveult *et al*, 2016). Gene ontology analysis was performed with David Bioinformatics Resource 6.8 (Huang *et al*, 2009).

Gene set enrichment analysis

GSEA (Subramanian *et al*, 2005) was obtained by comparing expression values of PCa spheres and PC3 cells of genes upregulated in PCa spheres ($P < 0.05$, $\log_2 FC > 1$). GSEA *P*-value was calculated over 100,000 permutations based on the phenotype, and FDR was < 25%.

Immunohistochemistry

Organoids were fixed using 4% paraformaldehyde (PFA) overnight and then washed with 70% ethanol. Fixed organoids were pre-embedded in HistoGel (Thermo Fisher Scientific) to pellet organoids together. Tissues and organoid pellets embedded in HistoGel were processed with an automated tissue processor and subsequently embedded in paraffin wax according to standard techniques. Samples were sectioned at 4 μm onto SuperFrost® Plus (Thermo Scientific) microscope slides and air-dried 37°C overnight. Immunohistochemistry was performed using BrightVision+ histostaining kit (Immunologic) according to manufacturer's protocol. Briefly, organoid sections were dewaxed in xylene (3× 3 min), followed by rehydration steps in descending percentages of EtOH (3 min in 100, 95, 90, 70, 50%), and washed twice in PBS. Slides were boiled in sodium citrate pH 6.0 (10 mM sodium citrate, 0.05% Tween 20) for 15 min and then allowed to cool to room temperature for 30 min. Slides were then washed in PBS and blocked for at least 1 h in PBS + 2% BSA. Samples were incubated with anti-Ki67 primary antibody (1:100, Abcam ab15580) overnight in blocking reagent at 4°C and then washed three times with PBS. Post-antibody blocking solution was added for 15 min, and samples were incubated at RT. Sections were washed twice with PBS and then were incubated for 30 min at RT with Poly-HRP-Goat anti-Mouse/Rabbit IgG. After incubation, sections were washed twice with PBS and were incubated with 3,3′ diaminobenzidine (DAB) mixture (Bright-DAB, Immunologic) for 8 min according to manufacturer protocol. After incubation, organoid sections were rinsed in deionized water and mounted with Fluoro-Gel.

Data availability

The datasets produced in this study are available in the following database: RNAseq and ChIP-Seq data: Gene Expression Omnibus GSE131268 (https://www.ncbi.nlm.nih.gov/geo/query/acc.cgi?acc=GSE131268).

Expanded View for this article is available online.

Acknowledgements

We thank Dominik Bär for technical assistance and Rostyslav Kuzyakiv for help in bioinformatic analyses. We thank Catherine Aquino and the Functional Genomic Center Zurich for the assistance in sequencing. This work was supported by the Swiss National Science Foundation (310003A-152854 and 31003A-173056), the National Center of Competence in Research RNA & Disease (funded by the SNSF), Forschungskredit of the University of Zurich (to M.R.), Sassella Stiftung (to S.C.F. and K.P.), Novartis, Julius Müller Stiftung, Olga Mayenfisch Stifung, Krebsliga Zurich, Swiss Cancer Research Foundation (KFS-3497-08-2014 and KFS-4527-08-2018-R), and ERC grant (ERC-AdG-787074-NucleolusChromatin).

Author contributions

RP-H and RS designed the study, made the figures, and wrote the article. RP-H performed the majority of the experiments and analyzed data. KP, SS, and RA performed analyses with organoids. SCF analyzed tumorspheres in the presence of inhibitors. MR and RA performed expression analyses with EP300 and BAZ2A inhibitors. JB analyzed BAZ2B in tumorspheres. LL provided bioinformatic support. RP-H, RA, and RS organized the structure of the manuscript. RS supervised and directed the study. All authors commented on the manuscript.

Conflict of interest

The authors declare that they have no conflict of interest.

References

Ahmed HU, Arya M, Freeman A, Emberton M (2012) Do low-grade and low-volume prostate cancers bear the hallmarks of malignancy? *Lancet Oncol* 13: e509 – e517

Asangani IA, Dommeti VL, Wang X, Malik R, Cieslik M, Yang R, Escara-Wilke J, Wilder-Romans K, Dhanireddy S, Engelke C *et al* (2014) Therapeutic targeting of BET bromodomain proteins in castration-resistant prostate cancer. *Nature* 510: 278

Ben-Porath I, Thomson MW, Carey VJ, Ge R, Bell GW, Regev A, Weinberg RA (2008) An embryonic stem cell–like gene expression signature in poorly differentiated aggressive human tumors. *Nat Genet* 40: 499

Berger MF, Lawrence MS, Demichelis F, Drier Y, Cibulskis K, Sivachenko AY, Sboner A, Esgueva R, Pflueger D, Sougnez C *et al* (2011) The genomic complexity of primary human prostate cancer. *Nature* 470: 214 – 220

Bray F, Ferlay J, Soerjomataram I, Siegel RL, Torre LA, Jemal A (2018) Global cancer statistics 2018: GLOBOCAN estimates of incidence and mortality worldwide for 36 cancers in 185 countries. *CA Cancer J Clin* 68: 394 – 424

Cancer Genome Atlas Research Network (2015) The molecular taxonomy of primary prostate cancer. *Cell* 163: 1011 – 1025

Cao H-Z, Liu X-F, Yang W-T, Chen Q, Zheng P-S (2017) LGR5 promotes cancer stem cell traits and chemoresistance in cervical cancer. *Cell Death Dis* 8: e3039

Chandran UR, Ma C, Dhir R, Bisceglia M, Lyons-Weiler M, Liang W, Michalopoulos G, Becich M, Monzon FA (2007) Gene expression profiles of prostate cancer reveal involvement of multiple molecular pathways in the metastatic process. *BMC Cancer* 7: 64

Chen P, Chaikuad A, Bamborough P, Bantscheff M, Bountra C, Chung C-w, Fedorov O, Grandi P, Jung D, Lesniak R *et al* (2015) Discovery and characterization of GSK2801, a selective chemical probe for the bromodomains BAZ2A and BAZ2B. *J Med Chem* 59: 1410 – 1424

Civenni G, Malek A, Albino D, Garcia-Escudero R, Napoli S, Di Marco S, Pinton S, Sarti M, Carbone GM, Catapano CV (2013) RNAi-mediated silencing of Myc transcription inhibits stem-like cell maintenance and tumorigenicity in prostate cancer. *Can Res* 73: 6816

Colombel M, Eaton CL, Hamdy F, Ricci E, van der Pluijm G, Cecchini M, Mege-Lechevallier F, Clezardin P, Thalmann G (2012) Increased expression of putative cancer stem cell markers in primary prostate cancer is associated with progression of bone metastases. *Prostate* 72: 713 – 720

Dann GP, Liszczak GP, Bagert JD, Müller MM, Nguyen UTT, Wojcik F, Brown ZZ, Bos J, Panchenko T, Pihl R *et al* (2017) ISWI chromatin remodellers sense nucleosome modifications to determine substrate preference. *Nature* 548: 607

de Dieuleveult M, Yen K, Hmitou I, Depaux A, Boussouar F, Dargham DB, Jounier S, Humbertclaude H, Ribierre F, Baulard C *et al* (2016) Genome-wide nucleosome specificity and function of chromatin remodellers in ES cells. *Nature* 530: 113 – 116

Denmeade SR, Isaacs JT (2002) A history of prostate cancer treatment. *Nat Rev Cancer* 2: 389 – 396

Drouin L, McGrath S, Vidler LR, Chaikuad A, Monteiro O, Tallant C, Philpott M, Rogers C, Fedorov O, Liu M *et al* (2015) Structure enabled design of BAZ2-ICR, a chemical probe targeting the bromodomains of BAZ2A and BAZ2B. *J Med Chem* 58: 2553 – 2559

ENCODE Project Consortium (2012) An integrated encyclopedia of DNA elements in the human genome. *Nature* 489: 57 – 74

Flemming A (2015) Targeting the root of cancer relapse. *Nat Rev Drug Discov* 14: 165

Fujisawa T, Filippakopoulos P (2017) Functions of bromodomain-containing proteins and their roles in homeostasis and cancer. *Nat Rev Mol Cell Biol* 18: 246

Gu L, Frommel SC, Oakes CC, Simon R, Grupp K, Gerig CY, Bär D, Robinson MD, Baer C, Weiss M *et al* (2015) BAZ2A (TIP5) is involved in epigenetic alterations in prostate cancer and its overexpression predicts disease recurrence. *Nat Genet* 47: 22 – 30

Huang W, Sherman BT, Lempicki RA (2009) Systematic and integrative analysis of large gene lists using DAVID bioinformatics resources. *Nat Protoc* 4: 44 – 57

Jin Q, Yu LR, Wang L, Zhang Z, Kasper LH, Lee JE, Wang C, Brindle PK, Dent SY, Ge K (2011) Distinct roles of GCN5/PCAF-mediated H3K9ac and CBP/p300-mediated H3K18/27ac in nuclear receptor transactivation. *EMBO J* 30: 249 – 262

Jurkowska RZ, Qin SU, Kungulovski G, Tempel W, Liu Y, Bashtrykov P, Stiefelmaier J, Jurkowski TP, Kudithipudi S, Weirich S *et al* (2017) H3K14ac is linked to methylation of H3K9 by the triple Tudor domain of SETDB1. *Nat Commun* 8: 2057

Karthaus W, Iaquinta P, Drost J, Gracanin A, van Boxtel R, Wongvipat J, Dowling C, Gao D, Begthel H, Sachs N *et al* (2014) Identification of multipotent luminal progenitor cells in human prostate organoid cultures. *Cell* 159: 163 – 175

Lasko LM, Jakob CG, Edalji RP, Qiu W, Montgomery D, Digiammarino EL, Hansen TM, Risi RM, Frey R, Manaves V *et al* (2017) Discovery of a selective catalytic p300/CBP inhibitor that targets lineage-specific tumours. *Nature* 550: 128 – 132

Leão R, Domingos C, Figueiredo A, Hamilton R, Tabori U, Castelo-Branco P (2017) Cancer stem cells in prostate cancer: implications for targeted therapy. *Urol Int* 99: 125 – 136

Lee KK, Workman JL (2007) Histone acetyltransferase complexes: one size doesn't fit all. *Nat Rev Mol Cell Biol* 8: 284 – 295

Leone S, Bär D, Slabber CF, Dalcher D, Santoro R (2017) The RNA helicase DHX9 establishes nucleolar heterochromatin, and this activity is required for embryonic stem cell differentiation. *EMBO Rep* 18: 1248 – 1262

Li H, Chen X, Calhoun-Davis T, Claypool K, Tang DG (2008) PC3 human prostate carcinoma cell holoclones contain self-renewing tumor-initiating cells. *Cancer Res* 68: 1820 – 1825

Li NA, Li Y, Lv J, Zheng X, Wen H, Shen H, Zhu G, Chen T-Y, Dhar S, Kan P-Y *et al* (2016) ZMYND8 reads the dual histone mark H3K4me1-H3K14ac to antagonize the expression of metastasis-linked genes. *Mol Cell* 63: 470 – 484

Li W, Ma H, Zhang J, Zhu L, Wang C, Yang Y (2017) Unraveling the roles of CD44/CD24 and ALDH1 as cancer stem cell markers in tumorigenesis and metastasis. *Sci Rep* 7: 13856

Li JJ, Shen MM (2018) Prostate stem cells and cancer stem cells. *Cold Spring Harb Perspect Med* 9: a030395

Li W, Middha M, Bicak M, Sjoberg DD, Vertosick E, Dahlin A, Häggström C, Hallmans G, Rönn A-C, Stattin P *et al* (2018) Genome-wide scan identifies role for AOX1 in prostate cancer survival. *Eur Urol* 74: 710 – 719

Liao Y, Smyth GK, Shi W (2013) The Subread aligner: fast, accurate and scalable read mapping by seed-and-vote. *Nucleic Acids Res* 41: e108

Liao L, Alicea-Velázquez NL, Langbein L, Niu X, Cai W, Cho E-A, Zhang M, Greer CB, Yan Q, Cosgrove MS *et al* (2019) High affinity binding of H3K14ac through collaboration of bromodomains 2, 4 and 5 is critical for the molecular and tumor suppressor functions of PBRM1. *Mol Oncol* 13: 811 – 828

Linder S, van der Poel HG, Bergman AM, Zwart W, Prekovic S (2018) Enzalutamide therapy for advanced prostate cancer: efficacy, resistance and beyond. *Endocr Relat Cancer* 26: R31 – R52

Luongo F, Colonna F, Calapa F, Vitale S, Fiori ME, De Maria R (2019) PTEN tumor-suppressor: the dam of stemness in cancer. *Cancers (Basel)* 11: 1076 .

Mayer MJ, Klotz LH, Venkateswaran V (2015) Metformin and prostate cancer stem cells: a novel therapeutic target. *Prostate Cancer Prostatic Dis* 18: 303

Mulholland DJ, Xin L, Morim A, Lawson D, Witte O, Wu H (2009) Lin-Sca-1+CD49fhigh stem/progenitors are tumor-initiating cells in the Pten-null prostate cancer model. *Cancer Res* 69: 8555 – 8562

Pattabiraman DR, Weinberg RA (2014) Tackling the cancer stem cells - what challenges do they pose? *Nat Rev Drug Discov* 13: 497 – 512

Phin S, Moore MW, Cotter PD (2013) Genomic Rearrangements of PTEN in prostate cancer. *Front Oncol* 3: 240

Pietrzak K, Kuzyakiv R, Simon R, Bolis M, Bar D, Aprigliano R, Theurillat JP, Sauter G, Santoro R (2020) TIP5 primes prostate luminal cells for the oncogenic transformation mediated by PTEN-loss. *Proc Natl Acad Sci USA* 117: 3637 – 3647

Plaks V, Kong N, Werb Z (2015) The cancer stem cell niche: how essential is the niche in regulating stemness of tumor cells? *Cell Stem Cell* 16: 225 – 238

Plaschkes I, Safran M, Twik M, Rosen N, Rappaport N, Nudel R, Hadar R, Fishilevich S, Iny Stein T, Cohen D *et al* (2017) GeneHancer: genome-wide integration of enhancers and target genes in GeneCards. *Database* 2017: bax028

Portillo-Lara R, Alvarez MM (2015) Enrichment of the cancer stem phenotype in sphere cultures of prostate cancer cell lines occurs through activation of developmental pathways mediated by the transcriptional regulator ΔNp63α. *PLoS One* 10: e0130118

Prager BC, Xie Q, Bao S, Rich JN (2019) Cancer stem cells: the architects of the tumor ecosystem. *Cell Stem Cell* 24: 41 – 53

Quinlan AR, Hall IM (2010) BEDTools: a flexible suite of utilities for comparing genomic features. *Bioinformatics* 26: 841 – 842

Raha D, Wilson TR, Peng J, Peterson D, Yue P, Evangelista M, Wilson C, Merchant M, Settleman J (2014) The cancer stem cell marker aldehyde dehydrogenase is required to maintain a drug-tolerant tumor cell subpopulation. *Can Res* 74: 3579 – 3590

Rajasekhar VK, Studer L, Gerald W, Socci ND, Scher HI (2011) Tumour-initiating stem-like cells in human prostate cancer exhibit increased NF-kappaB signalling. *Nat Commun* 2: 162

Ramirez F, Dundar F, Diehl S, Gruning BA, Manke T (2014) deepTools: a flexible platform for exploring deep-sequencing data. *Nucleic Acids Res* 42: W187 – W191

Rich JN (2016) Cancer stem cells: understanding tumor hierarchy and heterogeneity. *Medicine (Baltimore)* 95: S2 – S7

Robinson MD, Oshlack A (2010) A scaling normalization method for differential expression analysis of RNA-seq data. *Genome Biol* 11: R25

Robinson JT, Thorvaldsdottir H, Winckler W, Guttman M, Lander ES, Getz G, Mesirov JP (2011) Integrative genomics viewer. *Nat Biotechnol* 29: 24 – 26

Robinson D, Van Allen E, Wu Y-M, Schultz N, Lonigro R, Mosquera J-M, Montgomery B, Taplin M-E, Pritchard C, Attard G *et al* (2015) Integrative clinical genomics of advanced prostate cancer. *Cell* 161: 1215 – 1228

Santoro R, Li J, Grummt I (2002) The nucleolar remodeling complex NoRC mediates heterochromatin formation and silencing of ribosomal gene transcription. *Nat Genet* 32: 393 – 396

Saygin C, Matei D, Majeti R, Reizes O, Lathia JD (2019) Targeting cancer stemness in the clinic: from hype to hope. *Cell Stem Cell* 24: 25 – 40

Schmid MW, Grossniklaus U (2015) Rcount: simple and flexible RNA-Seq read counting. *Bioinformatics* 31: 436 – 437

Seiler D, Zheng J, Liu G, Wang S, Yamashiro J, Reiter RE, Huang J, Zeng G (2013) Enrichment of putative prostate cancer stem cells after androgen deprivation: upregulation of pluripotency transactivators concurs with resistance to androgen deprivation in LNCaP cell lines. *Prostate* 73: 1378 – 1390

Seim I, Jeffery PL, Thomas PB, Nelson CC, Chopin LK (2017) Whole-genome sequence of the metastatic PC3 and LNCaP human prostate cancer cell lines. *G3 (Bethesda)* 7: 1731 – 1741

Sheng X, Li Z, Wang DL, Li WB, Luo Z, Chen KH, Cao JJ, Yu C, Liu WJ (2013) Isolation and enrichment of PC-3 prostate cancer stem-like cells using MACS and serum-free medium. *Oncol Lett* 5: 787 – 792

Subramanian A, Tamayo P, Mootha VK, Mukherjee S, Ebert BL, Gillette MA, Paulovich A, Pomeroy SL, Golub TR, Lander ES *et al* (2005) Gene set enrichment analysis: a knowledge-based approach for interpreting genome-wide expression profiles. *Proc Natl Acad Sci USA* 102: 15545 – 15550

Tallant C, Valentini E, Fedorov O, Overvoorde L, Ferguson Fleur M, Filippakopoulos P, Svergun Dmitri I, Knapp S, Ciulli A (2015) Molecular basis of histone tail recognition by human TIP5 PHD finger and bromodomain of the chromatin remodeling complex NoRC. *Structure* 23: 80 – 92

Wang S, Garcia AJ, Wu M, Lawson DA, Witte ON, Wu H (2006) Pten deletion leads to the expansion of a prostatic stem/progenitor cell subpopulation and tumor initiation. *Proc Natl Acad Sci USA* 103: 1480 – 1485

Welti J, Sharp A, Yuan W, Dolling D, Nava Rodrigues D, Figueiredo I, Gil V, Neeb A, Clarke M, Seed G *et al* (2018) Targeting bromodomain and extra-terminal (BET) family proteins in castration-resistant prostate cancer (CRPC). *Clin Cancer Res* 24: 3149

Wong DJ, Liu H, Ridky TW, Cassarino D, Segal E, Chang HY (2008) Module map of stem cell genes guides creation of epithelial cancer stem cells. *Cell Stem Cell* 2: 333 – 344

Yadav SS, Stockert JA, Hackert V, Yadav KK, Tewari AK (2018) Intratumor heterogeneity in prostate cancer. *Urol Oncol* 36: 349 – 360

Yoshimoto M, Cutz JC, Nuin PA, Joshua AM, Bayani J, Evans AJ, Zielenska M, Squire JA (2006) Interphase FISH analysis of PTEN in histologic sections shows genomic deletions in 68% of primary prostate cancer and 23% of

high-grade prostatic intra-epithelial neoplasias. *Cancer Genet Cytogenet* 169: 128 – 137

Yu YP, Landsittel D, Jing L, Nelson J, Ren B, Liu L, McDonald C, Thomas R, Dhir R, Finkelstein S *et al* (2004) Gene expression alterations in prostate cancer predicting tumor aggression and preceding development of malignancy. *J Clin Oncol* 22: 2790 – 2799

Yu G, Wang L-G, He Q-Y (2015) ChIPseeker: an R/Bioconductor package for ChIP peak annotation, comparison and visualization. *Bioinformatics* 31: 2382 – 2383

Zhang Y, Liu T, Meyer CA, Eeckhoute J, Johnson DS, Bernstein BE, Nussbaum C, Myers RM, Brown M, Li W *et al* (2008) Model-based analysis of ChIP-Seq (MACS). *Genome Biol* 9: R137

Zhang CL, Huang T, Wu BL, He WX, Liu D (2017) Stem cells in cancer therapy: opportunities and challenges. *Oncotarget* 8: 75756 – 75766

Zhou Y, Grummt I (2005) The PHD finger/bromodomain of NoRC interacts with acetylated histone H4K16 and is sufficient for rDNA silencing. *Curr Biol* 15: 1434 – 1438